

Alkali and alkaline earth metals in liquid salts for supercapattery

Qiang Guo^{1,2,3}, Peiying Fan¹, Yuhan Zhang¹, Li Guan¹, Han Wang¹, Anna Croft^{1,4,*}, George Zheng Chen^{1,*}

¹ Department of Chemical and Environmental Engineering, Faculty of Engineering, University of Nottingham, Nottingham, NG7 2RD, U.K.

² Ningbo Institute of Materials Technology and Engineering, Chinese Academy of Sciences, Ningbo, 315201, P. R. China.

³ Department of Chemical and Environmental Engineering, Faculty of Science and Engineering, University of Nottingham Ningbo China, Ningbo, 315100, P. R. China

⁴ Department of Chemical Engineering, Loughborough University, Loughborough, Leicestershire, LE11 3TU, UK

ORCID:

Qiang Guo: 0000-0001-6373-5141

Peiying Fan:

Yuhan Zhang:

Li Guan: 0000-0001-6082-4886

Han Wang:

Anna Croft: 0000-0001-5330-150X

George Zheng Chen: 0000-0002-5589-5767

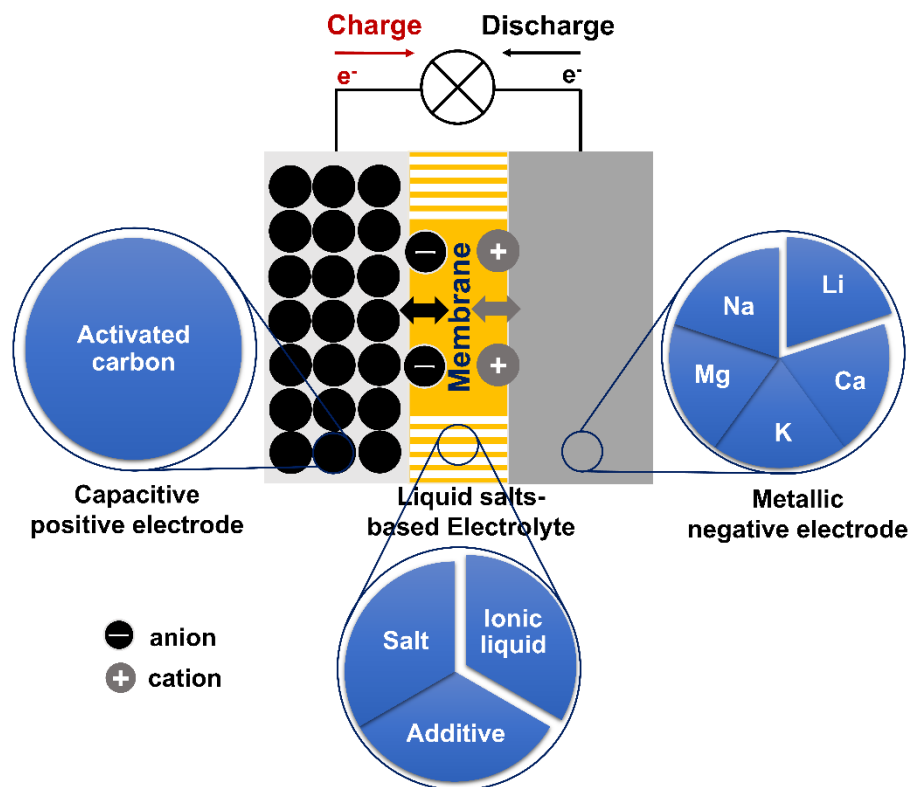
Correspondence emails:

a.k.croft@lboro.ac.uk (Anna Croft); george.chen@nottingham.ac.uk (George Chen)

ToC Text

Supercapatteries with liquid salts based electrolytes, battery negatodes of alkali or alkaline earth metals and supercapacitor positodes of high anodic stability are promising to outperform both rechargeable batteries and supercapacitors.

ToC Graphic



Abstract

The full oxidation of lithium metal ($4\text{Li} + \text{O}_2 \rightleftharpoons 2\text{Li}_2\text{O}$) offers a mass normalised Gibbs energy change greater than that for the combustion of carbon ($\text{C} + \text{O}_2 \rightleftharpoons \text{CO}_2$) or any hydrocarbon fuel ($\text{C}_n\text{H}_{2n+2} + (\frac{3n+1}{2})\text{O}_2 \rightleftharpoons n\text{CO}_2 + (n+1)\text{H}_2\text{O}$). This thermodynamic comparison promises a lithium-oxygen (air) battery with a petrol comparable energy density. Similar analyses apply to other abundant alkali and alkaline earth metals (AAEMs) which are all featured by their very high specific charge capacity and most negative electrode potentials. The success of lithium ion batteries (LIBs) in both research and commercial development confirms such thermodynamic predictions. However, the experimentally demonstrated energy capacities of all AAEM-based batteries are only small fractions of the thermodynamic values. A main cause is that a satisfactory oxygen positive electrode (positrode) is still to be developed, whilst the very few options of AAEM storage positrodes still do not match with AAEM negative electrodes (negatrodes) in charge capacity. Another challenge results from the complicated interactions between AAEMs and the currently used organic carbonate electrolytes that not only reduce the negatrode capacity but also exert restriction on both electron and ion transfers. The flammability of currently used organic electrolytes is another major concern on the safety of AAEMs batteries. Herein, we introduce the concept and potential, and review the relevant practices of a promising ionic liquid supercapattery that couples an AAEM negatrode with a supercapacitor positrode to bypass the thermodynamic and kinetic difficulties of an oxygen or AAEM storage positrode. The further discussion aims at the selection of ionic liquid-based electrolytes that can enable the reversible anodic dissolution of AAEMs and a wide potential window for the supercapacitor positrode. The use of molten salt-based electrolytes is also postulated and analysed, not only because of their high ionic conductivity, low cost and unique applications, but also their high temperatures that eliminate dendritic growth on the negatrode and heat buildup in the cell.

Key words: Supercapattery, supercapacitor, rechargeable battery, ionic liquid, molten salt, alkali metal, alkaline earth metal, positrode, negatrode,

Introduction

Driven by the rapid market expansion of portable electronics and electric transportation, the demand for cost-effective and high-efficiency energy storage has become increasingly important in the last two decades.¹ Electrochemical energy storage devices (EESDs), such as rechargeable batteries and supercapacitors are ideal candidates due to their modular nature, commercial attractiveness, and potential fossil-comparable energy capacity.

Commercial lithium (Li) ion batteries usually show satisfactorily high specific energy. Nevertheless, they demonstrate low power density due to the sluggish diffusion of Li ions in the intercalation-type electrode materials.¹ Especially, the fast intercalation of Li ions is not kinetically supported by the Li storage positive electrode (positrode) (LiCoO_2 or $\text{LiNi}_{1-x-y}\text{Co}_x\text{Mn}_y\text{O}_2$).² Moreover, because of their relatively low earth crust abundances, Co, Ni and Mn are or become very expensive, whilst their extraction from the respective minerals and decommission after service life exert a huge environmental impact and sustainability concern on the supply chains. Although, as a successful commercial product, the LiFePO_4 positrode shows improved thermal and chemical stability, cell safety, and longer cycle life, its moderate potential (<3.5 V vs. Li^+/Li) and high self-discharge rate only support a cell with relatively low exploitable energy density.³ On the other hand, traditional supercapacitors typically offer high power capability (e.g., 10 kW kg^{-1}) and long cycle life but only low to moderate specific energy ($<50 \text{ Wh kg}^{-1}$) due to the limited capacity for electrostatic adsorption and desorption of ions at the electrolyte | electrode interface.¹

Neither batteries nor supercapacitors alone can satisfy all the current and future commercial requirements. Thus, to achieve large energy capacity and high power capability in one EESD, hybrid devices combining capacitive and Nernstian charge storage mechanisms in the positrode and negative electrode (negatrode) without invoking Li intercalation have been proposed. Supercapattery (= **supercapacitor + battery**) is an innovative hybrid EESD, aiming to combine the advantages of rechargeable batteries and supercapacitors. Supercapatteries can provide sufficient electron transfer reactions and fast ion diffusion in the negatrode and positrode, thus showing higher power capability and longer cycle life than batteries, and larger energy capacity

than supercapacitors (Fig. 1).⁴ Accordingly, supercapatteries can be fabricated, for example, by pairing a supercapacitor positrode with a battery negatrode. The battery negatrode usually stores charge through the reversible transfer of localised valence electrons according to the Nernst equation, i.e., the Nernstian storage mechanism. In the supercapacitor positrode, the charge is stored via the EDL capacitance, pseudocapacitance, or even a combination of both mechanisms. The pseudocapacitance results from a capacitive Faradaic process according to the transfer of zone-delocalised valence electrons.⁴ The best performance of a supercapattery depends mainly on the optimal coupling of electrode materials and electrolytes to utilise effectively the potential windows and charge capacities of both electrodes without compromising the respective electron transfer kinetics and ion transport dynamics. While this coupling principle is further exemplified and discussed in the following sections, it is worth mentioning here that simply combining a Nernst electrode with a capacitive electrode does not necessarily lead to a better performing supercapattery. A key engineering strategy is to follow the two golden rules: the amount of charge, Q , and the amplitude of the current, I , passing through the two electrodes in a supercapattery (and any other EESD) must be equal.⁴

$$Q_n = m_n Q_{sp,n} = m_c C_{sp,c} \Delta E_c = Q_c \quad (1)$$

$$I_n = U / (R_n + R_c + R_{el}) = I_c \quad (2)$$

where m denotes the active mass on electrode, C the capacitance, I the current, U the cell voltage, R the resistance, and ΔE_c the working potential range of the capacitive electrode. The subscription n is for Nernstian, c for capacitive, sp for specific and el for electrolyte.

It should be noted that although R_{el} is the only term for electrolyte appearing in these two equations, the electrolyte also influences ΔE_c and U and both Q_n and Q_c . Also, for a given Nernstian electrode, Q_n is a constant, but Q_c is proportional to ΔE_c , which means U may be extended with using a smaller m_c as long as $\Delta E_c \leq \text{CPR}$, the capacitive potential range beyond which the electrode experiences Nernstian reactions. On the other hand, Nernstian electrodes have usually high values of $Q_{sp,n}$, particularly those based on alkali or alkaline earth metals (AAEMs), which means that the ratio $m_n/m_c (= C_{sp,c} \Delta E_c / Q_{sp,n})$ may be much smaller than 1. Therefore, if the positrode and negatrode masses of a supercapattery are made the same or similar as in the common practice in battery or supercapacitor manufacturing, the supercapattery may highly like underperform to its battery or supercapacitor counterpart.

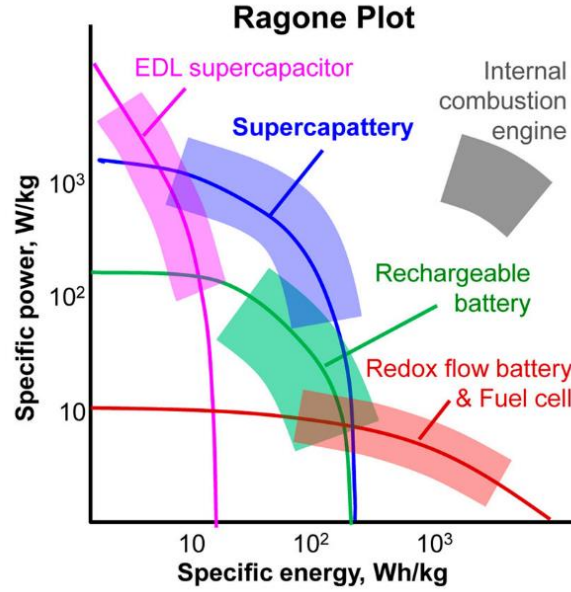


Figure 1. A schematic Ragone plot demonstrating the position of supercapattery in comparison with other energy devices.⁴

In principle, the energy capacity of any EESD can be calculated according to Eq. (3) in which U_{max} is the maximum cell voltage that is determined by the maximum potential difference between the positrode and negatrode.

$$W_{max} = \int_0^{U_{max}} i(t)U(t)dt \quad (3)$$

In rechargeable batteries, the positrode and negatrode potential windows are each relatively narrow and should be apart from each other as wide as possible to maximise the cell voltage. Unfortunately, this strategy also limits the minimum cell voltage to avoid over discharging. However, in supercapatteries, the capacitive electrode can have a very wide potential window that can overlap with that of the Nernstian electrode. As a result, supercapattery can be discharged to a practically meaningful low cell voltage, if not zero. Further, because of their narrow potential windows, the positrode and negatrode in a battery have to be matched carefully in mass loading to equalise the charge capacity. In a supercapattery, because the charge capacity of the capacitive electrode is a function of both mass loading and working potential range, there is a much larger space to manipulate the electrode mass loading for an optimal cell performance.

As a key component in EESDs, electrolytes keep electronic insulation but ionic conduction between, and assist charge transfer processes on the positrode and negatrode.⁵ In Eq. (3), U_{max}

can be the same as but not wider than the electrochemical stability window (ESW) of the electrolyte. Thus, electrolyte selection is a key design element and strongly determines the working or cell voltage of any EESD. It is particularly important for designing a supercapacitor whose linear voltage-charge relationship simplifies Eq. (3) to Eq. (4) below,

$$W_{max} = \frac{1}{2} C U_{max}^2 \quad (4)$$

where C is the capacitance and W_{max} is the maximum energy capacity of the supercapacitor (cell). Eq. (4) highlights the direct relevance of the supercapacitor performance with U_{max} which is limited by the ESW of the electrolyte. Aqueous, organic, and ionic liquids (ILs) electrolytes are all used in various EESDs. Although aqueous electrolytes exhibit high ionic conductivity and operational safety, the splitting voltage of water (1.23 V in theory at room temperature) has been widely viewed as a limit to the working voltage of aqueous cells. The working voltage of cells with traditional organic electrolytes can be extended beyond 3.0 V. However, several inevitable disadvantages like safety issues, maintenance difficulty, and high environmental impact due to their high volatility and flammability compromise the application of organic electrolytes in the EESDs.⁶ Therefore, there is a strong desire to develop new electrolytes to overcome these disadvantages.

In comparison with aqueous and organic electrolytes, ILs are pure liquid salts and widely recognized for their widest ESWs, more ionized environments, negligible volatility, low flammability, and high thermal, chemical, and electrochemical stabilities.⁷ However, ILs usually show ionic conductivity lower than 15 mS cm^{-1} at room temperature when they are viscous, which could lead to reduced achievable energy capacity and power capability in EESDs. Fortunately, many performance parameters of EESDs such as specific energy and power, or operation temperature can be further improved by employing mixed solvents of different ILs or ILs with organic solvent, or redox additives in IL electrolytes.⁸

Another key component in EESDs is electrode materials. In addition to the capacitance or charge capacity, the cell voltage of EESDs derived from the potential gap between negative and positive materials also greatly impacts the specific energy of EESDs. Thus, cell voltage should be given more attention. For example, it may be feasible to obtain a pseudocapacitive material with a specific capacitance value of 800 F g^{-1} , but it would be difficult to make a

symmetrical supercapacitor from such a material to approach a cell voltage of 3.0 V or higher. Thus, a unique strategy for improving the performance is to combine a supercapacitor positrode (either EDL capacitive or pseudocapacitive) with an AAEM negatrode of high theoretical specific capacity and very negative potential in a supercapattery with optimized IL electrolytes. For instance, Li metal, as the ultimate battery-type negatrode for high specific energy EESDs, is arousing a wide attention owing to its very negative potential (-3.04 V vs. standard hydrogen electrode) and high theoretical specific charge capacity (3860 mAh g^{-1}) and charge density ($2,061$ mAh cm^{-3}) as well as low mass density (0.53 g cm^{-3}).⁹⁻¹¹ The cell voltages of supercapatteries can be effectively broadened, which is beneficial to enhancing the energy storage capacity. A hypothetical supercapattery composed of a Li metal negatrode and a supercapacitor positrode of assumed 300 F g^{-1} is evaluated here. Considering that the specific charge capacity of Li metal (3860 mAh g^{-1}) is much larger than that of the supercapacitor electrode, the mass of the Li metal incorporated into the supercapattery can be negligible. The theoretical specific energy would be ~ 656 Wh kg^{-1} for a cell voltage varying from 4.0 V to 0.5 V. This theoretical value is even higher than that for conventional Li ion batteries (LIBs).⁵

Following the success of Li-based batteries, other AAEMs such as Na¹² or Mg¹³ have also been increasingly studied as the negatodes for batteries, mainly because of the concerns on the limited Li resources. A bottleneck in non-Li AAEMs ion batteries exists due to the lack of suitable positrode host materials⁸, but it may be easily bypassed by using a supercapacitor positrode to match the AAEMs negatrode. However, metal negatodes also suffer from a series of drawbacks, such as dendrite growth and unstable solid electrolyte interphase (SEI) formation, resulting in capacity fading, volume expansion, or poor power capability. Impressively, as electrolytes in AAEMs supercapatteries, IL engineering technology also shows promising advantages to alleviate the problems mentioned above. For example, key additives in IL are critical to **helping** metal-based cells achieve a stable reversible deposition. It was shown that novel non-flammable IL electrolytes composed of 1-ethyl-3-methylimidazolium and high-concentration bis(fluorosulfonyl)imide (FSI) with sodium **bis(trifluoromethanesulfonyl)imide** (NaTFSI) as a key additive could improve the Li metal deposition/dissolution behaviour. The formation of hybrid passivation interphases was found to contribute to dendrite-free Li deposition owing to the introduction of Na ions.¹⁴ Therefore, it seems that the ingenious design

of IL pairing with an AAEM negatode is key to enhancing the electrochemical performance of supercapatteries.

In this article, we first review the recent relevant research progress of IL-based electrolytes for typical AAEM supercapatteries, focusing on lithium (Li), sodium (Na), magnesium (Mg), potassium (K), and calcium (Ca). In the course of the discussion, we make necessary comparisons with AAEM ion supercapacitors and batteries. It is worth noting that many reported AAEM ion supercapacitors (e.g., Li-ion or Na-ion capacitors) are composed of an AAEM ion host electrode and an EDL capacitive or pseudocapacitive electrode. Because the ion host electrode works according to ion intercalation enabled redox chemistry, it is the same as a Nernstian or battery electrode. Thus, these ion capacitors are basically supercapatteries as well, although they are still different from those supercapatteries with a metal negatode.

We then discuss on the challenge and prospects for developing high-performance IL-based AAEMs supercapatteries. The focus is firstly on the unfavourable aspects of ILs, such as high viscosity caused low ionic conductivity, and corrosivity to metals. The AAEM negatodes also have intrinsic but problematic performances, mainly dendritic deposition and unwanted reactive interactions with ILs. Potential mitigations to such challenging issues are then sought from the literature and discussed.

In particular relevance to overcoming the low conductivity of ILs and dendritic deposition of AAEMs, we review the literature on batteries and supercapacitors with molten salts as the electrolyte, and then offer some preliminary considerations on the prospect of molten salt supercapatteries with an AAEM negatode. Molten salts, including molten hydroxides and oxides, are the high temperature counterpart of ionic liquids and they both are liquid salts in nature. (Another type of liquid salts is the so called deep eutectic solvents^{15, 16} whose application in EESD deserves a separate coverage.) They offer some unique advantages over ionic liquids. For example, LiCl (m.p. = 605 °C, b.p. = 1383 °C) remains stable in a very wide working temperature window from 650 °C to 1000 °C, which means a negatode of Li metal (m.p. = 180.5 °C) is in the liquid state, avoiding all problems associated with dendritic deposition. Further, at temperatures slightly higher than its melting point (e.g., by 50 °C), an inorganic molten salt becomes water-like in viscosity and hence offers high ionic conductivity, which is beneficial to high power capability. Last but not least, salt mixtures of inorganic and/or organic

natures often show eutectic melting behaviour, which lowers the working temperature. For example, the so called solar salt is used for heat transfer and storage in various concentrated solar power (CSP) plants. It is the mixture of NaNO_3 and KNO_3 with an equimolar eutectic temperature at about $222\text{ }^\circ\text{C}$, although the actual NaNO_3 content is higher on balancing the benefits from reduced cost, enhanced heat capacity and increased liquidus temperature.¹⁷⁻¹⁹

1. Ionic Liquid-based AAEM Supercapatteries

When the two electrode materials of an EEDS have been determined, the selection of electrolytes that are more suitable for each electrode material can greatly improve the cell stability and enable greater energy capacity and power capability.²⁰ Since its first report in 1994, the aqueous electrolyte of 5 M LiNO_3 for rechargeable lithium batteries has attracted a growing interest due to its cheap price, environmental friendliness, good conductivity, and easy preparation.²¹ The development of new aqueous electrolytes has been ongoing.²² In 2020, Adelowo et al.²³ developed a high-energy aqueous Li-ion on-chip capacitor based on interdigitated 3D carbon microelectrode arrays, which can achieve $5.03\text{ }\mu\text{Wh cm}^{-2}$ in areal energy, which is five times higher than other aqueous electrolytes. Organic electrolytes are often compared to aqueous electrolytes. The theoretical decomposition voltage of water is 1.23 V . Considering the overpotential of hydrogen or oxygen, the highest cell voltage of a traditional aqueous electrolyte is only about 2.0 V (such as that in lead-acid batteries). In LIBs, the operating cell voltage can be usually a high value between 3.0 and 4.0 V . Compared with aqueous electrolytes, organic electrolytes do not have advantages in price, availability, and conductivity, but can provide a wider and more stable ESW and wider temperature range (e.g., -30 to 70°C).²⁴ In recent years, the emerging sulfolane, ether and nitrile electrolytes have shown the potential to meet the requirements for high performance batteries.²⁵

Compared with aqueous and organic electrolytes, IL electrolytes have obvious advantages. As pure liquid salts at room temperature, they are highly ionized, negligibly volatile, non-explosive and non-flammable, and of great safety. Further, their ESWs can usually reach beyond 5.0 V .²⁶ For example, 1-butyl-1-methylpyrrolidinium bis(trifluoromethanesulfonyl)imide ($\text{Pyr}_{14}\text{TFSI}$) can remain stable up to 5.9 V as quoted by

Susantyoko et al.²⁷ Such wide ESWs are perhaps the most important reason for using ILs in supercapacitors against Eq. (4). However, unlike electrolyte with water and organic solvents of small molecules, ILs are mostly prepared from organic synthesis and present wide spectra of structures, compositions and properties. Thus, the understanding of charge (energy) storage mechanisms and performances derived mostly from aqueous and organic electrolytes in supercapacitors and consequently the manufacturing strategy may likely change when such new ILs become available. It has to be acknowledged that research on ionic liquids for supercapacitors has been growing fast and well covered in several recent reviews.^{6, 28-30} Considering space and topic, the following discussion will be based on selected literatures on ILs relevant to supercapatteries.

It is worth mentioning that ILs can be used not only directly as liquid electrolytes but also dissolve in traditional organic solvents or electrolytes to form new electrolytes with the merits of both. Such mixture electrolytes could achieve higher safety than organic electrolytes only, and better electrochemical performance than pure IIs.³¹ Fleischmann et al.³² developed high-pressure supercapatteries using 1-methyl-1-propylpyrrolidinium bis(trifluoromethanesulfonyl)imide (Pyr₁₃TFSI) as the electrolyte. This cell achieved 100 Wh kg⁻¹ in specific energy, 2 kW kg⁻¹ in specific power and over 1500 stable cycles, and could work satisfactorily at 80°C.³²

In addition, adding suitable redox agents to the electrolyte can also greatly improve the performance of electrochemical devices. Redox electrolytes of quinones dissolved in ILs enabled high-performance supercapatteries with energy densities three times higher than when ILs alone were used as electrolytes.³³ The current problem with IL electrolytes is that they may become cathodically unstable at potentials more negative than 1.0 V (vs Li/Li⁺), which could limit the voltage across the device to about 4.3 V. The ESWs of IL electrolytes are mainly affected by the nature of the solvent, conductive salts (i.e., cations and anions), and trace amounts of water and impurities. The cell voltage can be controlled by rationally adjusting these parameters.^{34,35} Furthermore, the high viscosity and low ionic conductivity of IL electrolytes are detrimental to the cycling stability and rate capability of hard carbons.

In the following sub-sections, centring on ILs-based AAEMs supercapatteries, we analyse typical examples of ILs-based AAEMs-ion supercapacitors, AAEMs batteries and AAEMs-ion

supercapatteries, and the impact of the cell configuration and electrolyte composition of these ILS-AAEMs based EEDS on the development of supercapatteries. The relevant electrode materials and electrolyte compositions and the respective electrochemical performances are summarised in Table 1. The order of introduction of these EEDS is lithium, sodium, magnesium, potassium, and calcium according to their atomic numbers in the periodic table.

1.1 . ILS in **lithium**-based supercapatteries

One of the first supercapatteries is the Li-ion-based battery-supercapacitor hybrid devices, invented by Amatucci and co-workers.³⁶ The negatode of the Li ion supercapattery was nanostructured $\text{Li}_4\text{Ti}_5\text{O}_{12}$, and the positrode was made of activated carbon (AC). This supercapattery could use either aqueous or organic electrolytes and was assembled using Li ion host materials as the positrode, such as Ti-based oxides,³⁷ Fe_3O_4 ,³⁸ Nb_2O_5 ,³⁹ and MnO .⁴⁰ However, due to the inherent disadvantages of the intercalation-type positrode, the reported Li ion supercapatteries still had the problem of slow energy storage kinetics, and the specific power and energy were limited within 900 W kg^{-1} and 40 Wh kg^{-1} , respectively.⁴¹

Li metal is considered the ultimate choice for the negatode of Li batteries due to its high theoretical capacity and extremely negative potential⁴², which is necessary for high energy EEDS.⁴³ **More recently**, designs that use Li metal as the negatode of supercapatteries have emerged. In 2021, Zhong et al.⁴⁴ first reported flexible Li metal capacitors with an *in-situ* prepared PETEA-based polymer gel electrolyte.⁴⁴ In the same year, Liu et al.⁴⁵ coupled a Li metal foil negatode with a three-dimensional scaffold activated carbon (3D-SAC) positrode into a cell with an organic carbonate electrolyte. The positrode showed a specific capacitance up to 280 F g^{-1} in a potential range from 1.5 to 4.3 V vs. Li/Li^+ . The galvanostatic charging and discharging (GCD) curve of the Li-carbon cell was very triangular in shape, similar to that of a capacitor thanks to the very flat GCD profile of the Li foil. A remarkable specific energy of 633 Wh kg^{-1} was derived from the GCD curve of the cell. It is noted that only the positrode mass was used to calculate the cell specific energy, which is still creditable because the mass change of the Li negatode should be insignificant compared to the total mass of the carbon positrode.

Table1. Summary of the electrode materials, the electrolyte composition, the configurations, and the electrochemical performances. (Configurations: 1. ILs-based AAEMs Supercapatteries 2. ILs-based AAEMs ion Supercapacitors 3. ILs-based AAEMs batteries 4. ILs-based AAEMs ion Supercapatteries)

Positrode	Negatrode	Ionic Liquid	Salt	Configuration	Cycle	CE (%)	Reference
N/S co-doped MESO	Na metal	Pyr ₁₃ -FSI	NaFSI	1	3000	100	46
LiMn ₂ O ₄	MESO	EMI-TFSI	LiTFSI	4	1000	100	47
LiNi _x Mn _{2-x} O ₄	MESO	EMI-TFSI	LiTFSI	4	1500	85	48
AC	Li ₄ Ti ₅ O ₁₂	Pyr ₁₃ -TFSI	LiTFSI	4	1500	70	32
LiNi _{1/3} Co _{1/3} Mn _{1/3} O	Li metal	Pyr ₁₄ -TFSI	LiTFSI	3	100	99	49
AC	Hard carbon	EMI-FSI	LiFSI	2	3000	95.33	50
AC	Hard carbon	Pyr ₁₃ -FSI	LiFSI	2	3000	88.44	50
PBA	K metal	EMI-Cl	EtAlCl ₂ and KFSI	3	820	99.9	51
Graphite	AC	Pyr ₁₄ -TFSI	Mg(TFSI) ₂	4	50	98	52
AC	Li metal	Pyr ₁₄ -FAP	LiClO ₄	1	-	-	5

Electrode materials: MESO, mesoporous carbon; AC, activated carbon; PBA, Prussian blue analogue.

Cations: Pyr₁₃, 1-methyl-1-propylpyrrolidinium; EMI, 1-ethyl-3-methylimidazolium; Pyr₁₄, 1-butyl-1-methylpyrrolidinium.

Anions: FSI, bis(fluorosulfonyl)imide; TFSI, bis(trifluoromethanesulfonyl)imide; FAP, tri(pentafluoroethyl)trifluorophosphate.

Salts: EtAlCl₂: ethylaluminium dichloride.

However, the Li dendrites formed during multiple charge and discharge cycles would pierce the separator and cause an internal short circuit of the EESDs. To solve this problem, several measures have been proposed, such as designing a highly stable artificial SEI between the metal electrode **materials** and the electrolyte to help Li metal deposit and dissolve more uniformly and prevent Li dendrites from piercing the separator.⁵³ Selecting appropriate electrolyte and electrolyte additives (e.g., NaTFSI),¹⁴ and developing new electrolytes are necessary to better prevent the generation of Li dendrites from the source.⁵⁴

The specific energy and power of supercapatteries with IL electrolytes have been demonstrated to be comparable to those using aqueous and traditional organic electrolytes, while maintaining excellent cycling stability.⁴⁷ To design the Li ion supercapattery, some studies have used mesoporous carbon as a capacitive electrode and 1.0 M lithium **bis(trifluoromethanesulfonyl)imide** (LiTFSI) in 1-ethyl-3-methylimidazolium **bis(trifluoromethanesulfonyl)imide** (**EMITFSI**) as the electrolyte. The positive electrode was LiMn_2O_4 (relevant electrochemical performance and electrode morphology are shown in Fig. 2).⁴⁷ The same research group also investigated the performance of a Ni-doped LiMn_2O_4 positive electrode in supercapatteries with a lithium salt/imidazolium IL electrolyte.⁴⁸

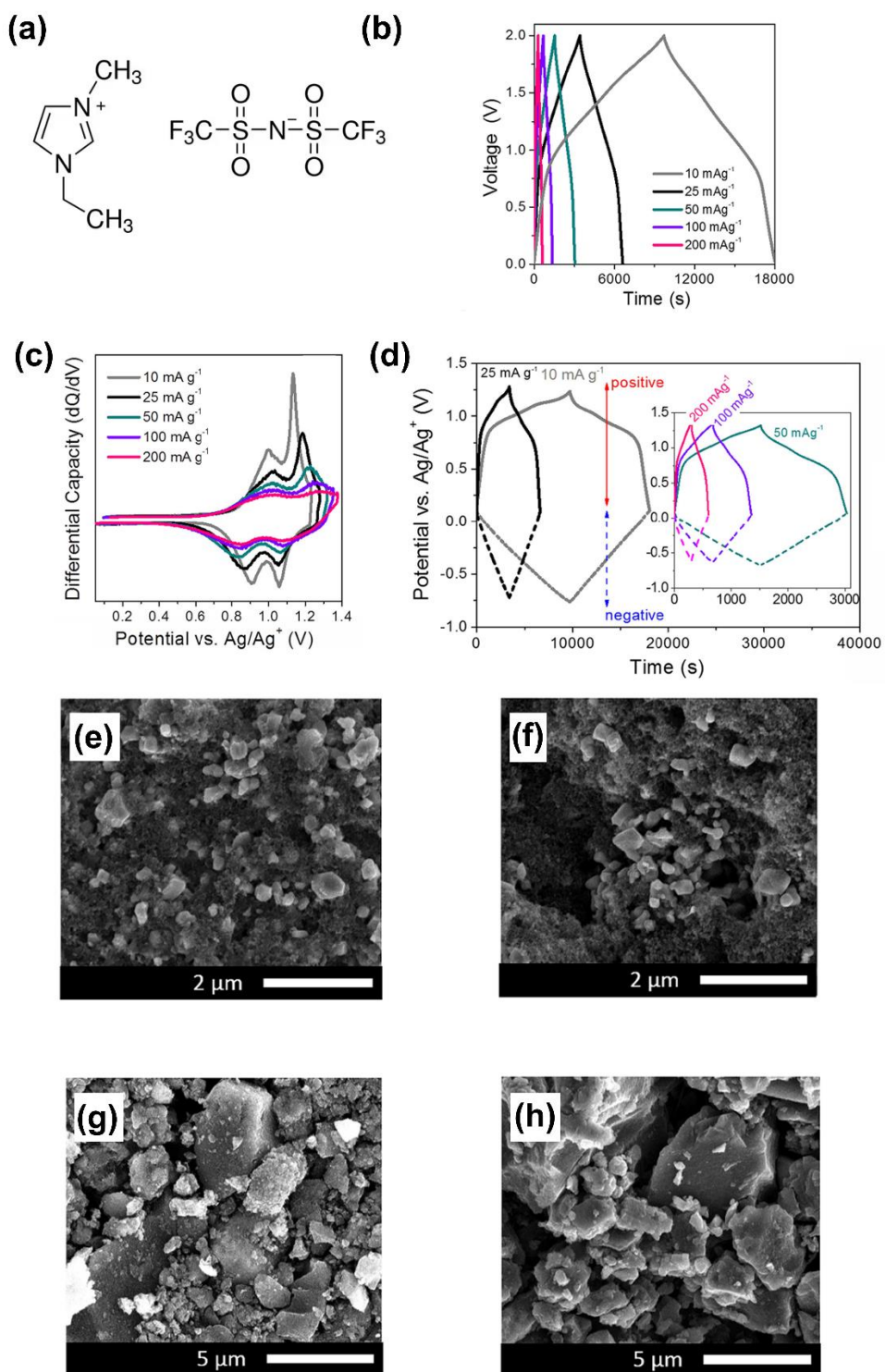


Figure 2. (a) molecular structures of cation and anion in the ionic liquid of 1-ethyl-3-methylimidazolium-bis(trifluoromethanesulfonyl)imide (EMITFSI). (b) Galvanostatic charge-discharge curves, (c) differential capacity vs. potential (dQ/dV) curves for the positrode, (d) evolution of the potentials of the electrodes at different current densities (10–200 mA g^{-1}) for $\text{LiMn}_2\text{O}_4||\text{MESO}$ cell in 1 M LiTFSI in EMITFSI. SEM images of

positrode: (e) before and (f) after cycling; SEM images of negatrod: (g) before and (h) after cycling.⁴⁷ (Reprinted from Ref. [47] with permission from Rightslink)

Fleischmann et al.³² used $\text{Li}_4\text{Ti}_5\text{O}_{12}$ as the negatrod, activated carbon as the positrod, and an IL containing Li salt as the electrolyte to form a supercapattery with a wide electrochemical window and a maximum voltage of 4.0 V. The reported EESD could achieve a specific energy of 100 Wh kg^{-1} and a specific power of 2 kW kg^{-1} (Fig. 3).

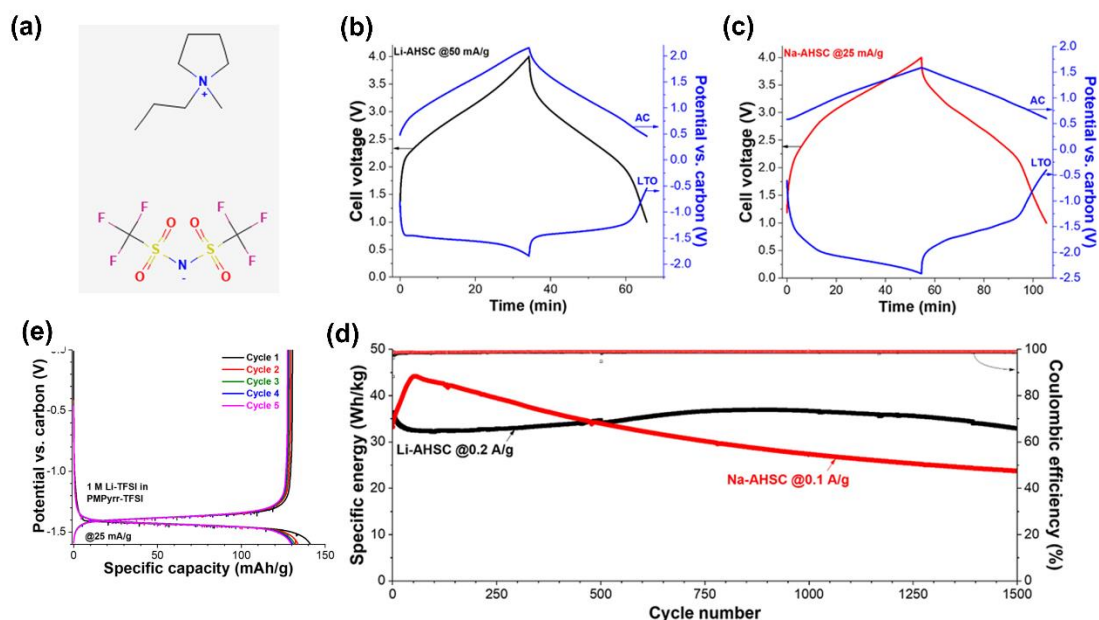


Figure 3. (a) 1-methyl-1-propylpyrrolidinium bis(trifluoromethanesulfonyl)imide ($\text{Pyr}_{13}\text{TFSI}$) ionic liquid molecular structure. Voltage profiles of (b) Li-based supercapatteries cycled at 50 mA g^{-1} and (c) Na-based supercapatteries cycled at 25 mA g^{-1} , including potential development at negatrod ($\text{Li}_4\text{Ti}_5\text{O}_{12}$) and positrod (activated carbon). (d) The cycling stability of Li-based supercapatteries cycled at 0.2 A g^{-1} , and Na-based supercapatteries cycled at 0.1 A g^{-1} over 1500 cycles between 1V and 4V cell voltage. (e) Comparison of first 5 galvanostatic cycles in 1 M LiTFSI in $\text{Pyr}_{13}\text{TFSI}$ electrolyte at 25 mA g^{-1} .³² (Reprinted from Ref. [32] with permission from Rightslink)

The first IL-based supercapattery with a Li metal negatrod and an activated carbon

positrode was reported in 2016 by our group.⁵ The electrolyte was a mixture of 1-butyl-1-methylpyrrolidinium tri(pentafluoroethyl)trifluorophosphate (**Py_{r14}FAP**) and gamma-butyrolactone (γ -GBL) (v/v-1/1) containing 0.5 mol L⁻¹ LiClO₄). The GCD curves of this IL cell were measured within a voltage range from 4.3 to 1.7 V and exhibited highly capacitive features, leading to a high specific energy of 232 Wh kg⁻¹ (Fig. 4). In the future, with the exploration of more positrode materials for IL-based supercapacitors and the development of Li metal as a negatrode technology for EESDs, the application of Li metal in supercapatteries with IL electrolytes is likely to achieve higher energy storage and more stable cycling performances.

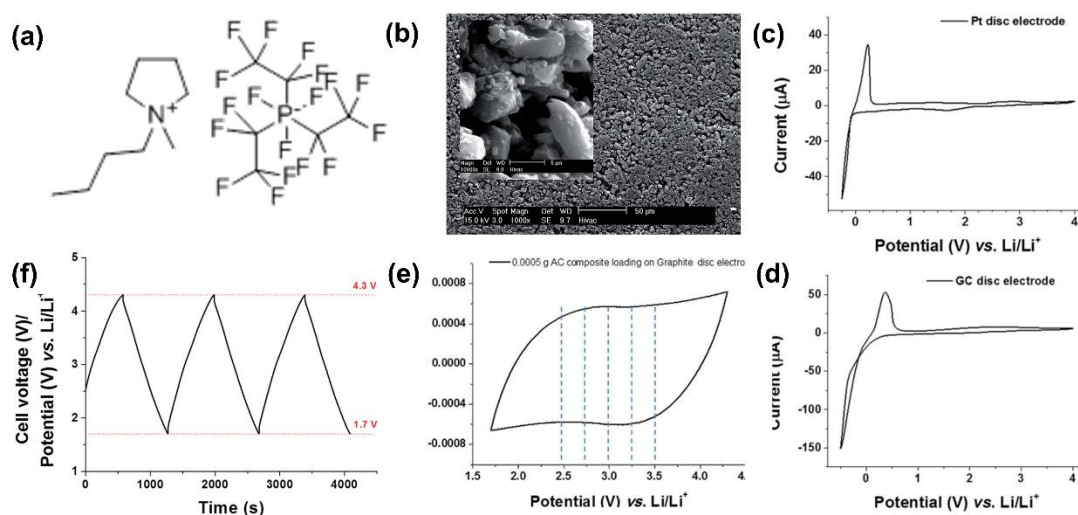


Figure 4. (a) 1-butyl-1-methylpyrrolidinium tri(pentafluoroethyl)trifluorophosphate (**Py_{r14}FAP**) ionic liquid molecular structure, (b) SEM images of the activated carbon pellet. The inset of (b) is high-magnification SEM images of AC pellet. Cyclic voltammetry curves using (c) a Pt disc electrode with 2 mm diameter and (d) a glass carbon disc electrode with 3 mm diameter, in a mixture of **Py_{r14}FAP** and γ -GBL, containing 0.01 mol L⁻¹ LiClO₄ at scan rate of 10 mV s⁻¹. (e) Cyclic voltammetry of 0.5 mg AC composite on a graphite disc electrode with 5 mm diameter in mixture of **Py_{r14}FAP** and γ -GBL, containing 0.5 mol L⁻¹ LiClO₄ at scan rate of 10 mV s⁻¹. (f) Galvanostatic charge–discharge curves of a pellet of 0.5 mg AC composite on a graphite disc electrode with 5 mm diameter in a mixture of **Py_{r14}FAP** and γ -GBL, containing 0.5 mol L⁻¹ LiClO₄. Current density: 1 mA cm⁻², Volume of **Py_{r14}FAP** and γ -GBL in the

mixture is 1: 1.⁵ (Reprinted from Ref. [5] with permission from Rightslink)

1.2. ILs in sodium-based supercapatteries

Li-based electrochemical devices occupy a leading position in the global EESDs market, but Li resources are not very abundant. In contrast, sodium (Na) resources are far greater than those of Li. Because the physical and chemical properties of Li and Na are remarkably similar, Na-based energy storage materials have become one of the candidates to replace or complement Li-based ones.⁵⁵ TiS_2 was the earliest reported reversible Na intercalation material.⁵⁶ Initially, considering the excellent performance of graphite electrodes in LIBs, scientists had tried but failed to use graphite as an intercalation material for Na-ion batteries.^{57, 58} In 2000, Stevens et al.⁵⁹ reversibly inserted Na^+ ions into hard carbon at room temperature and achieved a reversible Na capacity of 300 mAh g^{-1} . This is a big advance in the field of carbon-based Na intercalation materials, even if this value is lower than Li capacity of the same hard carbon.⁵⁹ In another study, an aqueous Na-ion capacitor with carbon microspheres as the negatrod and cobalt hexacyanoferrate (CoHCF , which is good AAEM ion host material) as the positrod achieved 54.4 Wh kg^{-1} in specific energy.⁶⁰

In order to obtain higher energy density, some scientists have proposed Na metal batteries with a theoretical capacity of about 1166 mAh g^{-1} .⁶¹ In 2019, a hybrid device composed of a Na metal negatrod and a capacitive material positrod was reported.⁶² The negatrod of this supercapattery was designed using a catalytic carbon nano template (C-CNTP), whose ordered graphitic structure enabled reversible Na metal deposition/stripping. The positrod employed nano porous pyroproteins (N-PPts) to store Na ions. The voltage window of such Na metal supercapatteries could reach 4.0 V which helped the delivery of high specific energy and power of 238 Wh kg^{-1} and 462 W kg^{-1} , respectively. In the following year, the same group developed another Na metal supercapattery based on a nano embossing pyropolymer catalytic layer (NE-P-CL) coupled with nanopore-engineered pyropolymer (NE-PP). In the new devices, NE-P-CL was designed for reversible Na deposition whilst NE-PP was fabricated as a

capacitive positrode. The cell exhibited high specific energy and power of 348 Wh kg^{-1} and 85.3 kW kg^{-1} , respectively.⁶³

At present, the difficulty encountered in the development of Na metal batteries is the high reactivity between metallic Na and electrolytes. In 2015, Iermakova and co-workers⁶⁴ reported the cyclic GCD profiles of Li/Li and Na/Na symmetrical cells in conventional alkyl carbonate electrolytes. Their observations revealed very large and electrolyte dependent resistance in the Na/Na cell (about 6 times larger than that of the Li/Li cell), indicating the formation of unfavourable and resistive SEI from reactions between Na and the carbonate electrolytes. Further, Na metal is fragile and difficult to process, whilst its low mechanical flexibility and poor electrolyte wettability compromise the interfacial stability. Thus, it is not easy to form a stable SEI at the “Na negatrode | carbonate electrolyte” interface,⁶⁵ which then leads to the growth of Na dendrites, the entry of free metallic Na into the electrolyte, and the hindrance of ion flux.⁶⁶

On the contrary, some IL electrolytes have been shown to be capable of offering much higher cycling stability than conventional electrolytes for Na metal deposition and dissolution. For example, using Na metal as the negatrode, N and S co-doped mesoporous carbon as the positrode, and the IL, 1-methyl-1-propylpyrrolidinium bis(fluorosulfonyl)imide (Pyr₁₃FSI) as the electrolyte, the supercapattery could stably cycle 3000 times at 100% coulombic efficiency (CE), and the capacity remains almost unchanged (Fig. 5).⁴⁶

1.3. ILs in magnesium-based supercapatteries

Unlike Li- and Na-based supercapatteries, magnesium (Mg) metal has unique advantages for use as the negatrode. Mg metal is an excellent negatrode material because it is neither as easy to form dendrites as Li metal nor as easy to react with an electrolyte as Na metal. In Mg supercapatteries, Mg metal and its alloys can be directly used as negatropes without an additional Mg metal pre-doping process. In 2014, Yoo et al.⁶⁷ developed, for the first time, a prototype Mg supercapattery as a successful

conceptual EESD. The negatrod of this supercapattery was a Mg foil and the positrod is made from a cloth of activated carbon. The problem of premature saturation of voids in AC, before the electrode potential reaches the limit, was solved by adding suitable electrolyte additives.⁶⁷

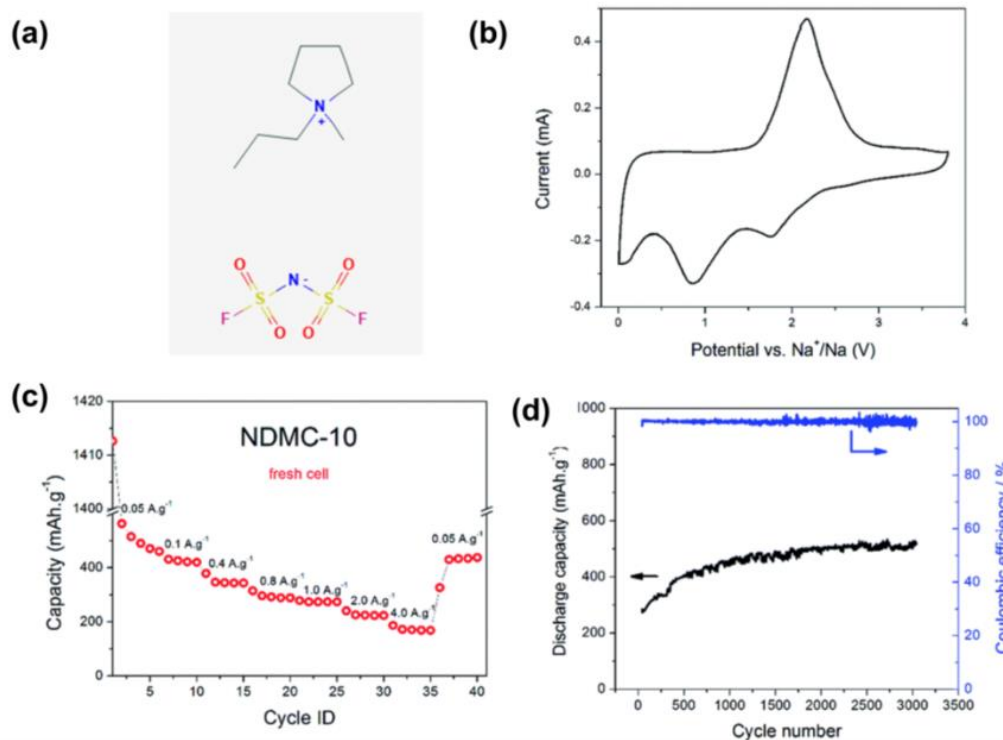


Figure 5. (a) 1-methyl-1-propylpyrrolidinium bis(fluorosulfonyl)imide (PyR₁₃FSI) ionic liquid molecular structure. (b) Cyclic voltammetry at 1 mV s⁻¹, (c) rate capability at different current densities and (d) long-term cycling (3000 cycles) at 1.0 A g⁻¹ of the ILs-based Na metal supercapatteries.⁴⁶ (Reprinted from Ref. [46] with permission from Rightslink)

However, it is known that the Mg²⁺ cannot penetrate the passivation film formed on the Mg metal negatrod, whilst reversible Mg deposition requires special electrolytes of Mg organo-haloaluminate complexes in ether solvents.⁶⁸ However, in such cases, the compatibility of every component of the electrolyte with the positrod material needs to be carefully considered. Complex electrolyte additives often make it difficult to match suitable positrod materials for existing Mg-based EESDs. The Mg

organo-haloaluminate electrolytes are often nucleophilic and can therefore chemically react with the electrophilic oxide positrode. Furthermore, the large ionic sizes of Mg ion complexes tend to limit the use of a porous carbon positrode in organo-Mg haloaluminate electrolytes.⁶⁷ Apparently, these non-ideal electrolytes are unfavourable for the development of Mg supercapatteries.

With the successive breakthroughs in high-power Mg metal batteries in the past two years, new ideas have emerged for solving problems in metal Mg supercapatteries. Meister et al.⁵² reported a novel dual-ion capacitor containing an IL electrolyte of magnesium bis(trifluoromethanesulfonyl)imide ($\text{Mg}(\text{TFSI})_2$) dissolved in 1-butyl-1-methylpyrrolidinium bis(trifluoromethanesulfonyl)imide ($\text{Py}_{14}\text{TFSI}$). When charging this device, the TFSI^- ion was stored in the graphite positrode through intercalation which is Faradaic (Nernstian) in nature, whilst Mg^{2+} and Py_{14}^+ ions were physically adsorbed/desorbed at the porous carbon negatrode in accordance with the EDL capacitive mechanism (Fig. 6). Obviously, this cell configuration falls in the scope of supercapattery.

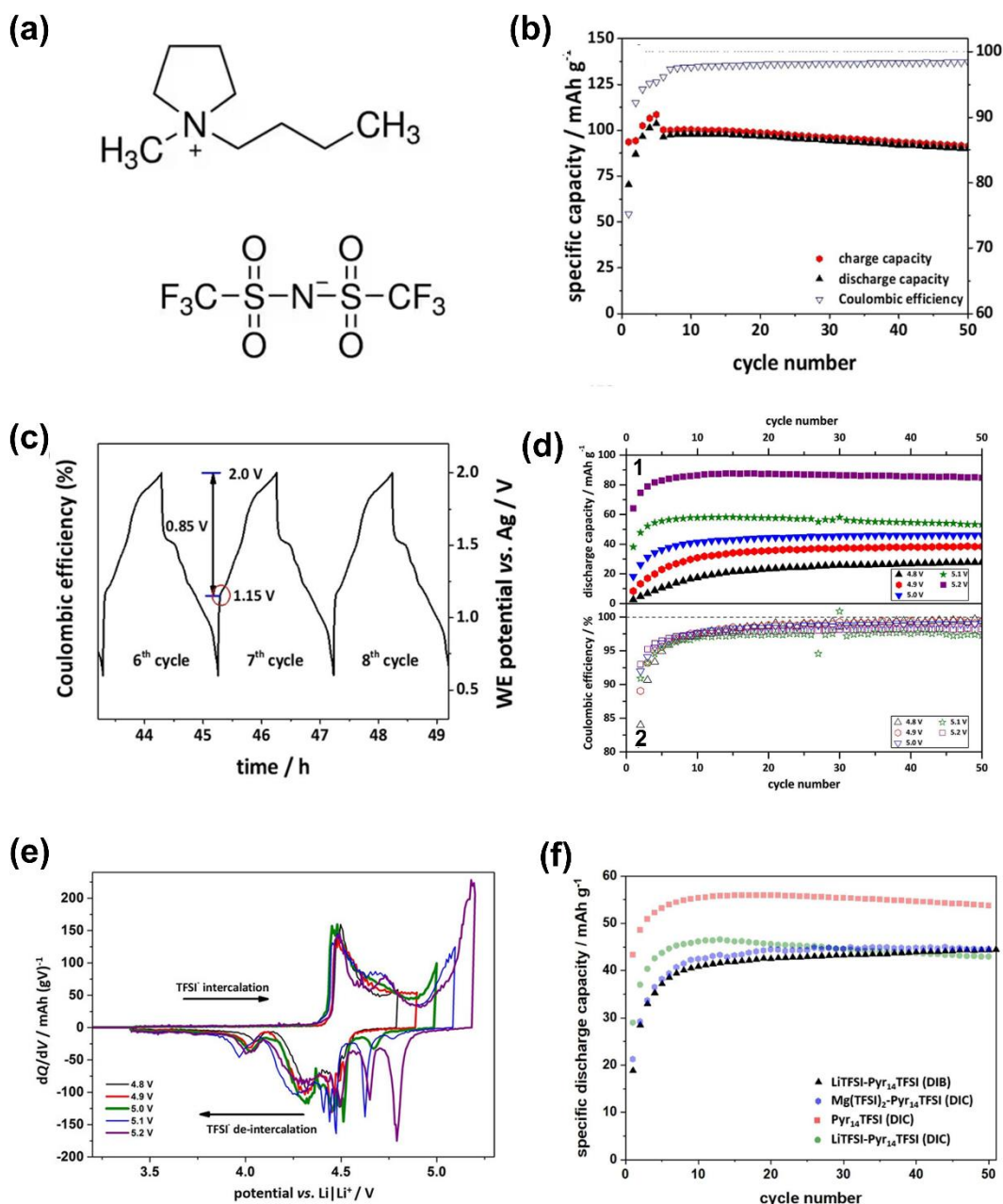


Figure 6. (a) 1-butyl-1-methylpyrrolidinium bis(trifluoromethanesulfonyl)imide (Pyr₁₄TFSI) ionic liquid molecular structure. (b) Cycling performances and (c) the related working electrode potential vs. time profiles of graphite||AC supercapattery during galvanostatic charge-discharge cycling at 100 mA g⁻¹. Electrolyte: 0.3 M Mg(TFSI)₂ in Pyr₁₄TFSI. (d) 1) Specific discharge capacities and 2) Coulombic efficiencies vs. cycle number and (e) comparison of specific differential capacity profiles (dQ/dV) of graphite||AC supercapattery at 50 mA g⁻¹. Potential range: 3.4 V to 4.8-5.2 V vs. Li/Li⁺; Electrolyte: 0.3 M Mg(TFSI)₂ in Pyr₁₄TFS. (f) Cycling

performances of graphite||AC supercapattery (DIC) at 50 mA g⁻¹ using either Pyr₁₄TFSI (red), 0.3 M LiTFSI in Pyr₁₄TFSI (green) or 0.3 M Mg(TFSI)₂ in Pyr₁₄TFSI (blue) as electrolyte. In addition, graphite || Li metal (DIB) cell (0.3 M LiTFSI in Pyr₁₄TFSI; black) at 50 mA g⁻¹ is illustrated. Potential range: 3.4 V to 5.0 V vs. Li/Li⁺.⁵² (Reprinted from Ref. [52] with permission from Rightslink)

In 2020, Yan and co-workers reported a high-power Mg battery based on a heterogeneous redox enolization mechanism and a weakly coordinated electrolyte. This work uncovered a positive reaction mechanism for rapid storage of Mg²⁺ ions, and at the same time invented a Mg electrolyte based on ether-mixed solvents and weakly coordinating anions (CB₁₁H¹²⁻), enabling Mg metal deposition with no dendrite formation at relatively high current densities, e.g., 20 mA cm⁻². The battery achieved 30.4 kW kg⁻¹ in specific power, which is almost two orders of magnitude higher than the highest power output of a previously reported Mg battery.⁶⁹

Furthermore, this work highlighted the discovery and application of a series of methoxyethylamine chelating agents that facilitate interfacial charge transfer kinetics in rechargeable bivalent metal batteries. The solvent shell recombination process can also suppress the side reactions occurring on the layered oxide positive electrode and metal negative electrode, leading to a rechargeable Mg metal battery with a specific energy of 412 Wh kg⁻¹.⁷⁰ Designing an artificial interface protective layer on the metal negative electrode not only effectively inhibited the harmful decomposition reaction of the common Mg electrolyte on the Mg metal negative electrode, but also promoted uniform Mg deposition, avoiding the occurrence of dendrite caused a short circuit in the battery.⁷¹ The development of electrode materials and electrolytes in batteries, capacitors, and supercapacitors is different but interlinked. Therefore, the development of Mg metal batteries is bound to bring new development opportunities for Mg metal supercapacitors.

1.4. Ions in potassium-based supercapacitors

In addition to Li, Na, and Mg, the other two relatively abundant AAEMs are

calcium (Ca) and potassium (K) which are also gradually emerging in research for using as the negatode in EEDSs. Relatively mature Li- and Na-based negatode materials and the matching electrolytes can form the base for the development of K- and Ca-based EEDS.⁷² In comparison with Li^+ , Na^+ and Mg^{2+} ions, both K^+ and Ca^{2+} are much larger in ionic radius, causing obvious volume change during charging and discharging, parasitic reactions, and dendritic growth. Whilst there are fewer studies reported on using Ca as the negatode.⁷³ K is clearly more popular in research, although the electrochemical devices are still far away from practical applications.

In 2020, Hundekar et al.⁷⁴ achieved *in-situ* healing of dendrites in K metal batteries by rationally controlling the self-heating behaviour of K electrodes. This opens the door to K supercapatteries with high energy density.⁷⁴ Fabrication of metal K-containing negatodes by infiltrating aligned carbon nanotube membranes with molten K was attempted to provide sufficient electrode/electrolyte contacts for charge transfer. Such a K metal negatode showed stable plating/stripping profiles and low polarisation during charge and discharge. In addition, this design could also effectively suppress the growth of dendrites. It was paired with a Prussian blue positrode when assembled into a full cell whose very good performance confirmed a high compatibility between these two electrode materials.⁷⁵ This approach was also considered as an effective solution for the design of K metal negatodes.

In recent years, the use of IL electrolytes for high-performance K-based batteries has gradually increased. In 2019, Yoshii et al.⁷⁶ developed the $\text{Pyr}_{13}\text{TFSI}$ -based stable and safe IL electrolytes with potassium bis(trifluoromethanesulfonyl)imide (KTFSI) to work with new high voltage layered positrode materials for high-voltage K-ion batteries. In 2020, Sun et al.⁵¹ reported a battery using an IL, 1-ethyl-3-methylimidazolium chloride with two important additives, i.e., potassium bis(fluorosulfonyl)imide (KFSI) and EtAlCl_2 , as the electrolyte and metal K as the negatode (Fig. 7). The IL electrolyte specified was found to be able to provide a robust K-containing passivating interphase in batteries to achieve excellent cycle performance.

In the same year, a unique potassium monocation ionic liquid (K-SCIL) was developed in Japan for use in K-ion batteries. The IL electrolyte worked well with the

graphite negatrod and supported high current densities.⁷⁷ Even though no supercapattery that combines K metal or K ions with IL electrolytes has been reported yet, with the research on high-quality positrod materials and functional ILs, there will be more and more K-based supercapatteries based on ILs in future research.

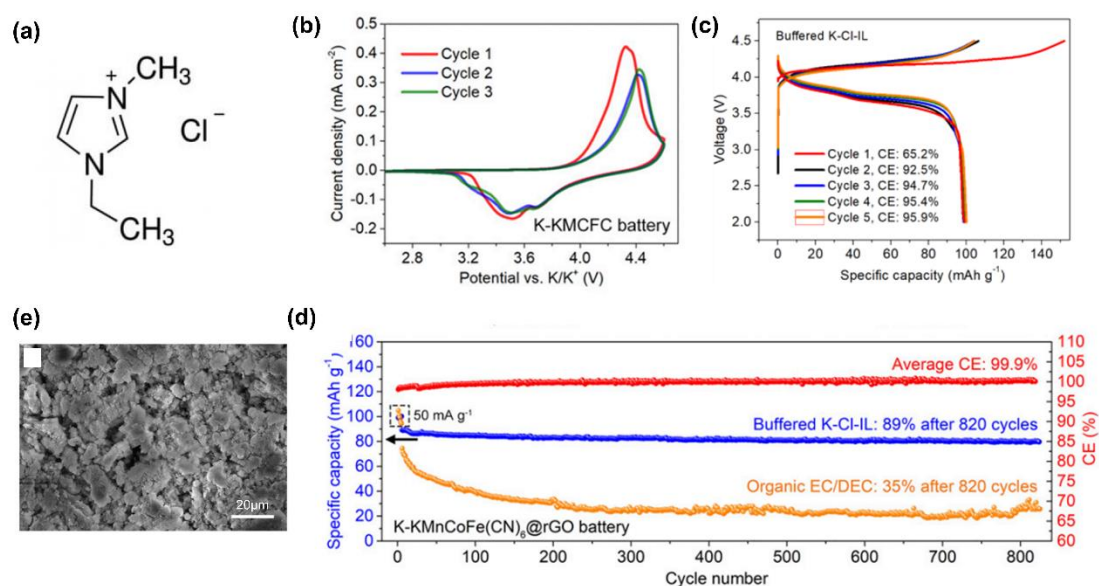


Figure 7. (a) Molecular structure of 1-ethyl-3-methylimidazolium chloride (EMICl) ionic liquid. (b) Cyclic voltammetry curves of a K metal || KMCFC battery using buffered K-Cl-IL electrolyte at a scan rate of 0.1 mV s⁻¹. (c) The initial five galvanostatic charge-discharge curves of K metal || KMCFC@rGO batteries at 50 mA g⁻¹ using buffered K-Cl-IL electrolyte. (d) Cycling performances of K metal || KMCFC@rGO batteries using buffered K-Cl-IL and organic electrolytes at 100 mA g⁻¹. (e) SEM images of a K negatrod cycled in a K metal || KMCFC@rGO cell. EtAlCl₂ and KFSI were added in a mixture of AlCl₃ and EMICl at a molar ratio of 1.2, to obtain the final KCl-buffered chloroaluminate IL (buffered K-Cl-IL) electrolyte. KMCFC represents K_{1.90}Mn_{0.92}Co_{0.08}[Fe(CN)₆]_{0.96} and reduced graphene oxide was introduced KMCFC (referred to as KMCFC@rGO).⁵¹ (Reprinted from Ref. [51] with permission from Copyright (2020), National Academy of Sciences)

1.5. ILs in calcium-based supercapatteries

Calcium (Ca) is considered as a promising metal for rechargeable batteries due to its theoretically very negative working potential. However, the passivation layer formed on the Ca metal surface in the proton electrolyte cannot effectively conduct Ca^{2+} , making the deposition process difficult to achieve. In addition, it is difficult to find electrode materials for Ca EESDs that can efficiently store and release Ca reversibly.⁷⁸ Recently, to address this issue, Park et al.⁷⁹ applied density functional theory (DFT)-based high-throughput quantum mechanical calculations to predict the battery-related properties of various layered materials incorporating Ca and transition metal oxides. CaCo_2O_4 was most recently found to have an optimal balance of properties including thermodynamic stability, average voltage, energy density, and synthesisable properties.

The direct use of metallic Ca as the negatode is far from meeting the performance standards of commercial batteries because the coulombic efficiency of the Ca metal negatode was found to be unsatisfactory at low power.

Optimization of the SEI structure via tuning IL is an effective way to enhance the coulombic efficiency of Ca-based batteries. Recently, Passerini et al.⁸⁰ achieved an extraordinary initial discharge capacity of 332 mAh g^{-1} and reversible capacity of 244 mAh g^{-1} using the optimized IL-based electrolyte ($[\text{Ca}(\text{BH}_4)_2]_{0.05}[\text{N}_{07}\text{TFSI}]_{0.95}$) in V_2O_5 || Ca cells. It was revealed by quantitative analysis that the polyether chains could effectively replace TFSI^- from the Ca^{2+} coordination sphere, fostering the reversible Ca deposition/dissolution process. Meanwhile, an organic-rich, but inorganic-poor SEI layer was formed, enabling Ca^{2+} diffusion rather than passivating the Ca metal. Among the Ca-based EESDs that have been reported so far, the best performer is a supercapattery in which tin which is capable of alloying with Ca was used as the negatode and activated carbon as the positrode.⁸¹ It exhibited a fairly large reversible capacity of 92 mAh g^{-1} , unrivalled rate capability (full recovery of the discharge capacity upon rate variation), and high capacity retention of 84% after 1000 cycles at room temperature. Among the IL electrolytes for Ca-based EESDs, $\text{Pyr}_{14}\text{TFSI}$ and $\text{Pyr}_{\text{H}_4}\text{TFSI}$ based IL electrolytes showed good transport performance and

electrochemical stability in EDL capacitors. However, the compatibility of such electrolytes with the TiS_2 positrode is not optimistic, which makes the application of IL electrolytes in Ca-based energy storage devices still a big challenge.⁸²

2. Challenges and Prospects

In this part, the current main challenges in terms of ILs and AAEMs negatropes for developing the respective supercapatteries are discussed. The prospects of developing high-performance IL-based AAEMs supercapatteries are also analysed and speculated.

2.1. Challenges

2.1.1. Ionic liquids

ILs are completely composed of anions and cations and show liquid-like properties at, or around room temperature ($<100^\circ\text{C}$).⁸³ The high physical and chemical stability of ILs are the key to their successful application in AAEMs supercapatteries. First of all, in terms of electrochemical inertness, they have a wide electrochemical window and strong anti-oxidation and anti-reduction ability, and hence can effectively improve the output cell voltage and the overall energy capacity of AAEMs supercapatteries. In terms of thermal stability, ILs are mainly non-volatile and non-flammable, which provides the best choice for improving safety performance. AAEMs negatropes usually involve polymorphous deposition upon dis-/charging. Unfortunately, the non-uniform metal deposit can easily cause the cell to short circuit and undergo thermal runaway. Compared with organic solutions, IL electrolytes further alleviate this thermal runaway and prevent explosion/combustion behaviour. In terms of structural characteristics, ILs are also known as “designer green solvents”. The synthesis of ILs with targeted performances can be achieved by designing and adjusting anions and cations, resulting in improved electrochemical performance.

However, low ionic conductivity, possible risk of leakage to the environment, high selectivity to material structure/composition, strong corrosivity, and unsatisfactory

functionality are currently the main challenges for their use in AAEMs supercapatteries.

The design via synthesis and selection of appropriate additives in the IL electrolyte are important ways to modify and improve any undesirable physical and chemical properties of IL, e.g., low ionic conductivity.⁸⁴ First of all, low ionic conductivity at room temperature, owing to high viscosity, sometimes results in reduced energy capacity and power capability in AAEMs supercapatteries. Modification of the cation structure, e.g., replacing the linear alkyl substituents of the ammonium cation with curled ether groups, was shown to significantly lower the viscosity of the ILs with the same anion by a factor of 0.2 to 0.1.⁸⁵

The addition of some molecular solvents in IL electrolytes can also effectively improve their ionic conductivity.⁸⁶ Lalia et al.⁸⁷ developed a new binary mixture of non-flammable additives composed of triethylphosphate (TEP) and ethylene carbonate (EC) to improve the performance of IL electrolytes. After adding TEP and EC in the 0.4 M LiTFSI in *N*-methyl-*N*-propylpiperidinium bis(trifluoromethanesulfonyl)imide (PP₁₃TFSI), the ionic conductivity at room temperature was enhanced from 8.2×10^{-4} S cm⁻¹ to 3.5×10^{-3} S cm⁻¹. No change in the ESW of PP₁₃TFSI was observed. Novel anion and cation designs are an effective alternative strategy to modify the low ionic conductivity of ILs. Chen et al.⁸⁸ fabricated a novel IL of 1-trimethylsilylmethyl-3-butylimidazole bis(trifluoromethanesulfonyl)imide ([SiM-BIM]TFSI) for Li metal rechargeable batteries. Imidazolium cation with a silicon-containing substituent could reduce the viscosity and improve the ionic conductivity of IL electrolytes. Further, the heteroatom Si substituent was found to make the C-2 position of the imidazolium cation less active, which stabilised the cation against cathodic polarisation. This effect in turn helped uniform Li deposition/dissolution and contributed to increasing the CE and stability of the cell.

Many ILs themselves are unfriendly or even harmful to the environment and must be fully confined within the EESDs during their whole service life. The liquid nature of ILs means high mass mobility which makes it challenging to achieve full utilisation efficiency during long-term dis-/charging cycling. At any level, the loss of IL will not only increase the cost but also lower the energy capacity of the EESDs, or even bring

about the risk of leakage beyond the legal limits. Compared with traditional organic electrolytes, polymer electrolytes have the advantages of no flow and no leakage. Thus, by combining ILs and polymer materials, the leakage and utilisation issues are in principle resolved, whilst the conductivity, stability and safety of polymer electrolytes are also improved. Rupp et al.⁸⁹ combined polyethylene oxide (PEO), 1-butyl-1-methylpyrrolidinium bis(trifluoromethanesulfonyl)imide (Pyr₁₄TFSI), and LiTFSI into PEO/IL/LiTFSI ternary composites. Not only was the conductivity increased, but also the safety issues associated with LIBs were improved. Lavall et al.⁹⁰ obtained a new electrolyte based on thermoplastic polyimide esters with different proportions of LiTFSI, propylene carbonate (PC) and *N*-ethyl(methylether)-*N*-methylpyrrolidinium bis(trifluoromethanesulfonyl)imide (RYRA₁₂₀₁TFSI). These polymer electrolytes showed good thermal stability, wide ESWs and a maximum ionic conductivity of 10⁻⁴ S cm⁻¹.

Sometimes, large IL ions effectively block the pores in different ways, including size mismatch and strong/permanent adsorption that hinder further ion movement in and out of the pores. Thus, ILs may perform a high selectivity towards the structure of positrode/negatrode materials (e.g., surface area, pore size or porosity). Shiraishi et al.⁹¹ discussed the electrochemical capacitance of activated carbon fibres in 1-ethyl-3-methylimidazolium tetrafluoroborate (EMIBF₄) versus a propylene carbonate solution of 0.5 M (C₂H₅)₄NBF₄ (TEABF₄/PC). The activated carbon fibres showed a very stable cycling performance but decreased capacitance due to the mismatch between the micropore sizes of the activated carbon fibres and the TEA⁺ cation in TEABF₄/PC. Activated carbon fibres showed a higher capacitance in EMIBF₄, but its cycle performance was relatively poor because of a mismatch between the narrow micropores and the size of EMI⁺ ion. The analysis showed that the EMI⁺ cation could strongly adsorb on a flat carbon surface. Therefore, in the slit-shaped micropores of the activated carbon fibres, EMI⁺ ions could irreversibly adsorb on the walls of the micropores. As a result, the discharge capacity decayed fast. Complementary to the pore size, the positrode must have a sufficiently large number of pores to maintain an adequate number of the redox species and the products (from the charging reaction) inside the

pores for improving the Nernstian charge storage.⁹²

Some halides in ILs show strong corrosion to the current collector, which can affect the practical application of IL in EESDs. IL-based electrolytes have been studied for secondary Al batteries as early as 1933⁸³ and recently gained increasing attention in Al metal batteries. A special issue with Al batteries is that the SEI layers which can form during dis-/charging often passivate the Al surface, both ionically and electrically. While, surface passivation of Al can be alleviated using ILs containing AlCl₃ according to the work from Jayaprakash et al.⁹³ Thus, Al ion conductivity in SEI can be improved using this reported IL. However, the Cl in the Al salts (Al₂Cl₇⁻) is quite corrosive, even to stainless-steel current collectors.⁹⁴ In addition, the chlorine in Mg organohaloaluminate salts (among other variants) is very corrosive to the current collectors.⁹⁵ Therefore, when selecting the anions of ILs, their corrosiveness to battery components should be carefully considered, especially in practical applications. In addition, necessary anti-corrosion measures should be taken. For example, an anti-corrosion coating may be sprayed on the surface of battery components e.g., current collectors to effectively reduce the corrosive effects of ILs.

The thermochemical and electrochemical stability of ILs is one of the basic reasons why they are regarded as excellent green solvents and electrolytes. However, high stability also means poor functionality for some specific tasks, but it can be altered or improved by the addition of other additives, salts and/or solvents. For instance, redox additives or mediators can be dissolved in the IL electrolyte to improve the energy capacity of EESDs, particularly supercapacitors. Such additives undergo reversible electron transfer reactions inside a porous electrode and can contribute to extra charge storage capacity.^{92, 96} Further, the ionic conductivity of IL electrolytes can be enhanced to a certain degree with the addition of ionic redox additives, which improves the specific power of EESDs.^{97, 98}

Navalpotro et al.³³ dissolved 0.4 M *para*-benzoquinone (*p*-BQ) in 1-butyl-1-methylpyrrolidinium bis(trifluoromethanesulfonyl)imide (Pyr₁₄TFSI). This redox IL was used in asymmetrical hybrid supercapacitors (which were in principle the same as supercapatteries). One pair of very broad redox current peaks appeared on the CV (Fig.

8a) in a symmetrical two-electrode cell with vulcan carbon and commercial activated carbon electrodes, indicating the presence of a Faradaic contribution from the redox processes of *p*-BQ.

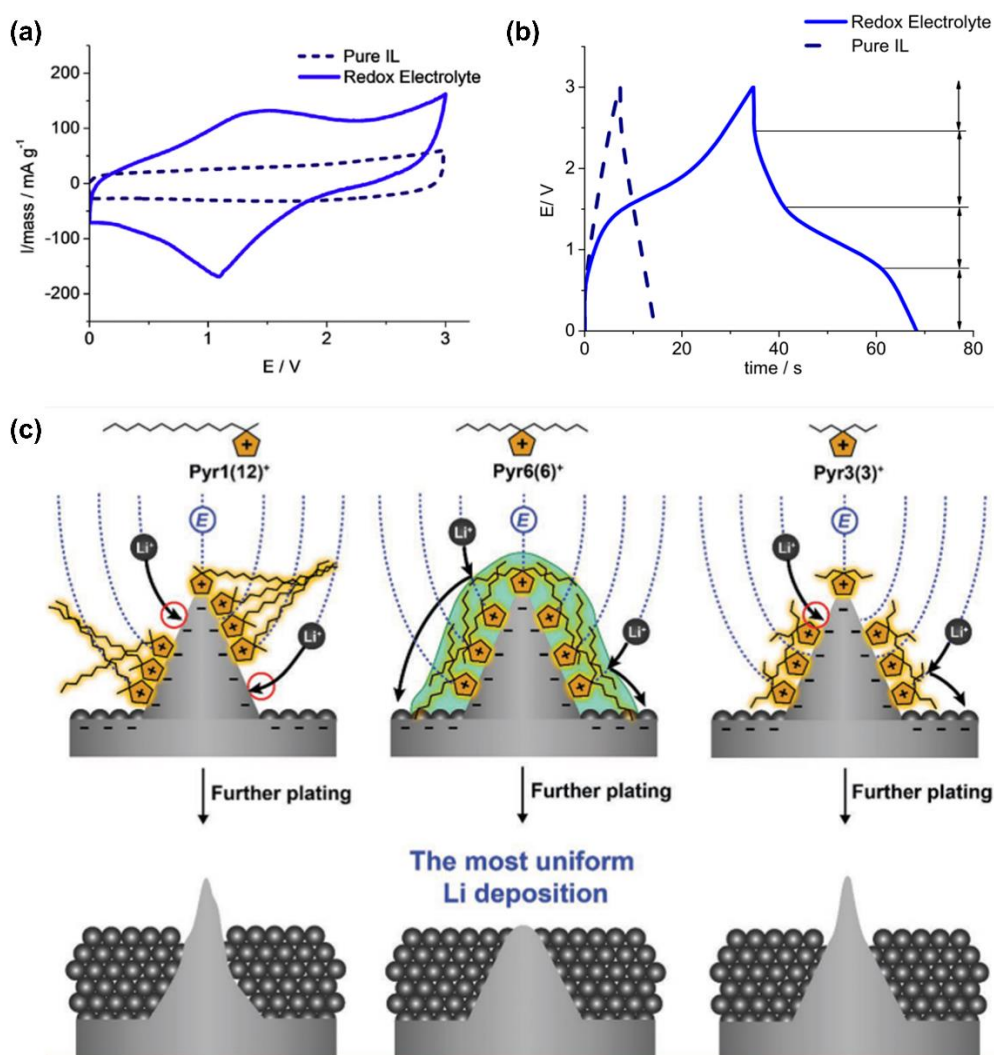


Figure 8. (a) Cyclic voltammograms and (b) Galvanostatic charging and discharging profiles up to 3.0 V of a symmetrical cell of vulcan carbon. Electrolytes: Redox IL electrolyte of 0.4 M *p*-BQ in PYR₁₄TFSI (solid blue lines) and pure PYR₁₄TFSI (dashed black lines). Temperature: 60°C. Current density: 10 mA cm⁻².³³ (c) The impact of three different IL cations, Pyr1(12)⁺ (left), Pyr₆(6)⁺ (middle), and Pyr₃(3)⁺ (right), on inducing uniform Li metal deposition owing to the formation of lithiophobic protective layers on Li protuberances.⁹⁹ (Reprinted from Ref. [33] and Ref. [99] with permission from Rightslink)

The GCD profiles as shown in Fig. 8b illustrated approximately four different regions, including the plateau region typical of faradaic contribution between 1.5 and 0.8 V during discharging. These CV and GCD features show that charge storage in the vulcan carbon-based supercapacitors is composed of the EDL capacitance and Faradaic reactions (Nernstian process). The specific energy of the cell with the redox IL operating at different working voltages (2.0, 3.0, and 3.5 V) was obviously greater than that with pure PYR₁₄TFSI. Interestingly, the specific energy of vulcan carbon (240 m² g⁻¹ in a specific area) was more significant than pica carbon (2400 m² g⁻¹) with or without using the same redox IL. This feature also confirms that the effectiveness of applying redox ILs is strongly influenced by electrode materials and structures.

Some special physical and chemical properties of ILs can significantly improve the electrochemical performance of AAEMs, especially for metal deposition on the negatodes without dendritic growth.^{100, 101} ILs with an appropriate Li salt concentration can effectively improve the stability of the electrode interface. A solution of 2 M LiTFSI in 1-methyl-1-propylpyrrolidinium bis(trifluoromethanesulfonyl)amide (Pyr₁₃TFSI) with added ether solvent to form a hybrid IL electrolyte was reported by Li et al.¹⁰² Li dendrite growth and the corrosion of Li metal in the batteries was effectively alleviated by surface passivation in this hybrid IL electrolyte. They found that there was a synergistic effect of Pyr₁₃TFSI IL and Li salt remarkably enhancing the reversibility of Li plating. The stability of SEI layers, including passivation substances (Li₃N and LiF) on Li metal, can be dramatically improved by including Pyr₁₃TFSI in the electrolyte.

Targeted designs for anions and cations are also an important strategy to improve battery performance. For instance, cations with lithiophobic symmetric alkyl chains were introduced to 1,1-dihexylpyrrolidinium bis(fluorosulfonyl)imide ([Pyr₆(6)FSI]) to shield this moiety from the Li negatode (Li tips) and mitigate the continuous growth of Li dendrites by Jang et al.⁹⁹. This effect could have resulted from firstly pyrrolidinium cations (Pyr⁺) being preferentially attracted to the protuberances on the Li surface by the electric field and secondly the reduction potential of Pyr⁺ was more negative than that of the Li ions (-3.04 V vs standard hydrogen electrode, SHE). In other words, the

Pyr⁺ cations with symmetric alkyl chains led to the most densely assembled shielding layer compared with the conventional cations with asymmetric alkyl chains (Fig. 8c). Thus, alkyl chains in this cation enabled the cation to be assembled on protuberant tips, forming a protective layer against further Li deposition. Uniform Li deposition and higher CE become more realistic by this protective layer on any protuberances on the surface of Li deposit.⁹⁹

2.1.2. AAEMs Negatodes

The use of AAEM negatodes can be traced back to the early work on the potential of Li metal electrode material by Lewis in 1913.¹⁰³ The use of a Li metal electrode was limited by safety issues and cycling decay, preventing its practical application for rechargeable Li metal batteries at that time. The Li negatode was then abandoned when Sony commercialized LIBs with a carbon negatode in 1991.¹⁰⁴ However, with the explosive development of modern science and technology, the requirements of EESDs with high specific energy and high power capability are gradually increasing, and conventional LIBs and supercapacitors¹⁰⁵⁻¹⁰⁷ cannot meet such fast growing requirements. Supercapatteries combining the merits of capacitive and Nernstian charge storage mechanisms in the positrode and negatode can in principle offer the solution. Combining a supercapacitor positrode with an AAEM negatode of high theoretical capacity and much negative potential (Fig. 9) in supercapatteries with an optimised IL electrolyte may be an ideal strategy to further improve energy storage performances.¹⁰⁸

The demand for high energy storage capacity in LIBs has revitalised research on AAEMs negatodes. Unfortunately, two electrochemical challenges strongly limit the practical application of a pure AAEM negatode in EESDs. One is the plating properties of the AAEMs negatode material. The other is the nature of the electrolyte decomposition on the AAEMs negatode.¹⁰⁹

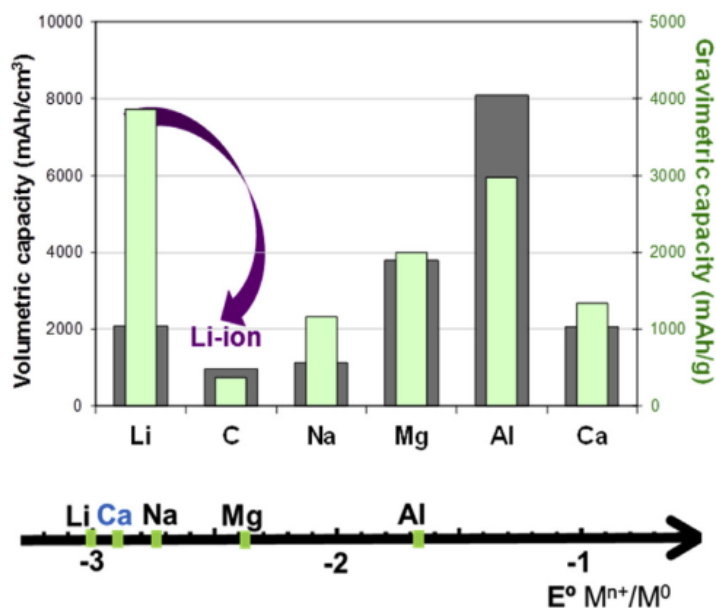


Figure 9. Comparison of the standard reduction potential versus the charge density (left, volumetric capacity) or specific charge capacity (right, gravimetric capacity) for different metals and graphite in the LIB.¹⁰⁸ (Reprinted from Ref. [108] with permission from Rightslink)

Dendrite formations are relatively common on many metal negatrodes. For example, Li metal batteries were plagued with well-known dendrite formation that can lead to thermal runaway or explosion.¹¹⁰ Compared with Li metal, Na or K metal batteries will likely result in even more dangerous thermal-runaway accidents due to the combination of higher reactivity and lower melting point of Na and K metals.¹¹¹ In addition to the safety issues related to dendrite formation, continuous exposure to fresh metals can lead to electrolyte decomposition and then capacity loss, resulting in electrolyte depletion and low CE. The severity of these issues is strongly related to the operating conditions (e.g., current density, areal capacity, and electrolyte composition) and most vitally, the nature of the AAEM negatrode.¹¹²

Solid electrolyte interphase (electrolyte decomposition)

The SEI as a passivation film on the metal negatrode can isolate the continuous direct contact between the electrolyte and the metal and provide channels for the

transport of desolvated ions. Thus, it must be carefully designed.¹¹³ Although stable SEI formation with the same level of performance as that in LIBs is difficult to obtain on Li, other AAEMs negatodes seem to be more problematic than the Li negatode. For instance, stable SEI cannot be formed on the Na metal owing to the bulky and porous nature of the SEI formed in carbonate-based electrolytes, which will enhance the direct contact between the Na negatode and the electrolyte.¹¹⁴ Furthermore, the SEI on the Na metal is more soluble in carbonate electrolytes due to the higher number of inorganic species and weaker ionic bonds (larger ionic radius) in SEI compared with that on the Li metal.¹¹⁵ Diglyme-based electrolytes can facilitate the formation of higher inorganic material and minimal polymeric film, inducing improved electrochemical performance of Na metal batteries owing to the decreased SEI solubility in the ether-based electrolyte.¹¹⁶

The dication of Mg¹¹⁷ or Ca¹¹⁸ suffers from great difficulty in diffusing through the SEI layer. For the SEI on Mg and Ca, the metal is not only electrically passivated but also ionically insulating, which greatly restricts the transfer of both cations and electrons.¹⁰⁹ For this reason, Mg Grignard reagents were developed as an electrolyte that does not decompose over Mg in the Mg metal battery. Thus SEI-free Mg can be formed during cycling.¹¹⁹ Later, Mg organohaloaluminate salts-based electrolytes were developed by Aurbach et al.,¹²⁰ which can render the electrolyte sufficiently stable toward Mg metal to enable pairing with a positrode and facilitate stable Mg ion conductive SEI formation.

The highly tuneable properties of ILs have given rise to very specific electrolyte compositions. Specifically, ILs in Mg batteries need to be functionalized with ether to facilitate stable stripping and plating. Without the ether solvent, the Mg²⁺ dication is coordinated with the bis(trifluoromethanesulfonyl)imide (TFSI) anion. The chance of TFSI reduction and Mg passivation film formation is significantly increased during plating Mg because of the close proximity between the TFSI anion and the Mg atom.¹²¹ Interestingly, recent work demonstrated that pre-fabricated artificial SEI coatings composed of cyclised polyacrylonitrile and Mg(CF₃SO₃)₂ over Mg could improve the Mg²⁺ ion conductivity to $1.19 \times 10^{-6} \text{ S cm}^{-1}$, while remaining electronically

insulating.¹²² This work can further allow the use of a wide range of electrolyte solvents.

The commercial availability of Ca metal batteries is still unknown, possibly due to the highly reactive nature of Ca and relatively low specific energy estimation, which has attracted limited research on such EESDs.¹²³ However, according to a recent breakthrough, reversible plating of Ca with $\text{Ca}(\text{BH}_4)_2$ in a tetrahydrofuran (THF) electrolyte was achieved for ~50 cycles,¹²⁴ where a CaH_2 layer formed on the surface of Ca served as a poor-quality SEI. More impressively, a recent work on the Ca metal negatrod showed that the SEI formed on Ca could conduct Ca^{2+} ions at mild temperatures ranging from 75 to 100°C, enabling an extended range of applications.¹²⁵

Polymorphous metal deposit (plating properties)

The formation of polymorphous metal deposits, e.g., dendrites, is a common phenomenon in many electrochemical metal plating processes. Generally, there are four different modes of electrodeposition: root growth (whiskers), tip growth (dendrite), a combination of root and tip growth, and higher-dimensional plating (non-dendritic growth).¹²⁶ Many efforts have been devoted to suppressing the formation of dendrites, such as electrolyte engineering,¹²⁷ artificial SEI or coating layer,^{9, 128} and development of 3D current collectors.^{129, 130} Fundamentally, metal electrodeposition consists of five sequential processes. First, the metal ions transfer from the bulk electrolyte. Secondly, desolvation of the metal ion from the electrolyte occurs. The process of surface adsorption is followed by charge transfer and ultimately surface diffusion to the deposition site. The final morphology and quality of metal deposit are affected by each of these steps.¹³¹

There are three modes describing polymorphous metal growth, as shown in **Fig. 10a**. For example, for Li, these are whisker-like (Li whisker) growth, mossy-like (Li moss) growth, and tree-like (Li dendrite) growth. These each follow different growth patterns. Li whiskers follow a root growth pattern because there is no compressive stress whilst electronic/ionic conductivities are higher at the root. Li moss belongs to the surface growth pattern because of a higher deposition rate than SEI formation. Li dendrites follow a tip growth pattern due to the higher electric field at the tips.¹³²⁻¹³⁴

Mossy metal usually forms before Li whiskers or serious Li dendrite growth and originates from the difference in the SEI layer's electronic conductivity.

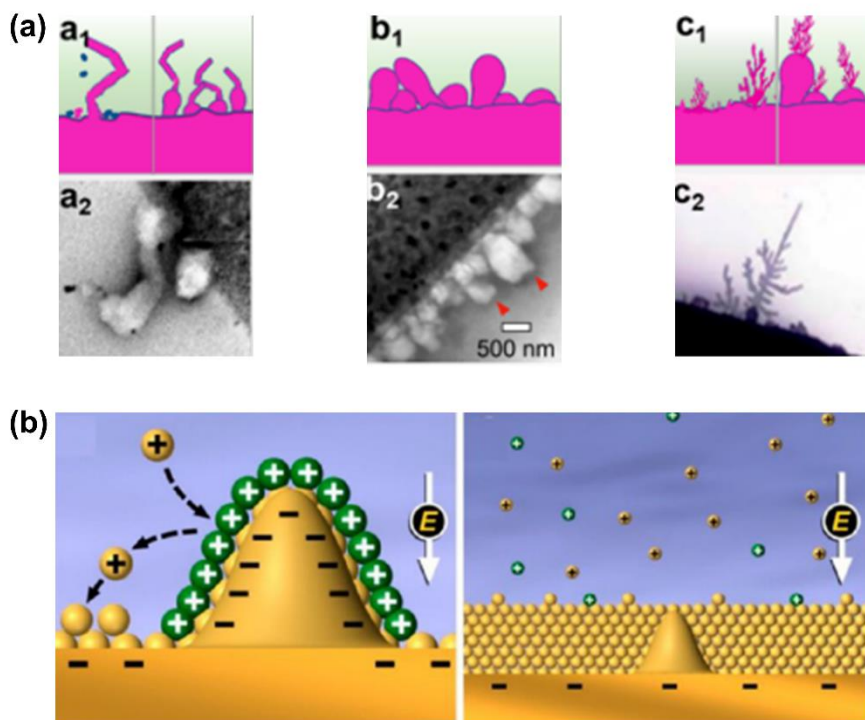


Figure 10. (a) Three modes describing polymorphous Li metal growth: (a1, b1, and c1) schematic morphologies, (a2, b2, and c2) real microscopic images for whisker-like, mossy-like, and tree-like (dendrite) deposits.¹³² (b) Diagram of Li deposition based on the self-healing electrostatic shield mechanism.¹³⁵ (Reprinted with permission from [132]. Copyright 2021, Reprinted with permission from ref. [135]. Copyright 2013, American Chemical Society.)

Interestingly, almost no mossy dendrite growth on multivalent AAEMs negatodes has been found, possibly because of the lack of special SEI that can induce mossy growth.¹⁰⁹ The most noteworthy property of Mg negatodes is their dendrite-free deposition. A possible reason may be the surface energy of Mg being larger than that of alkali metals ($\text{Li} > \text{Na} > \text{K}$).¹³⁶ This explanation is in agreement with DFT calculations and experimental results which indicate that Mg does not plate dendritically (large surface area) due to the higher surface energy relative to Li.^{137, 138} However, it was

reported that the absence of dendrites in Mg might not be an inherent property arising from surface energy, but rather a result of surface diffusion of Mg atoms.¹³⁹ The surface diffusion of Mg atoms on an Mg bulk surface was calculated as relatively faster than that of Na and Li.¹⁴⁰ Thus, slower surface diffusion can lead to tip growth. To alleviate this dendrite growth, electrolyte/metal ion pairings with faster surface diffusion could be implemented.

Metal ions in the electrolyte are not fast enough to match the electron flux at currents beyond a certain limiting level and deposition time, causing severely polarised potential in cells.¹⁴¹ The metal plating switches from high-dimensional or mossy plating to tip dendritic growth. At Sand's time (dendrites formation time), the concentration of the cation for plating is zero at the metal surface and pure dendritic growth begins.¹⁴² The electrolyte cannot supply sufficient cations for plating, and sharp dendrites are rapidly formed to maintain a constant current density. The presence of a 3D current collector is reported to effectively decrease the current density and prolong Sand's time, alleviating dendrite formation.¹²⁹ Enhancing salt concentration can decrease the local spatial charge variation and mitigate dendrite formation owing to the increased plating cation's transference number (Li¹⁴³, Na¹⁴⁴, and K¹⁴⁵). However, high viscosity and related slow charge and mass transfer at a higher current are the main problems, especially in IL electrolytes. Another alternative method is to add small amounts of cations such as Cs⁺ with a more negative effective reduction potential relative to Li, to reduce variations in spatial charge (Fig. 10b).¹³⁵

2.2. Prospects

2.2.1. Room temperature approach

The design strategies for AAEM negatropes in IL and organic electrolytes for room temperature uses can be summarised as (1) faster surface diffusion on the metal negatropes, (2) better transport properties in the electrolyte, and (3) stable SEI layers on AAEM negatropes.^{146, 147} All types of dendritic deposits should be eliminated to facilitate AAEM supercapatteries commercialization. Strategies should focus on

increasing lateral surface diffusion (alleviating tip growth) and improving ionic transportation properties (alleviating space-charge effect) of the IL electrolytes to mitigate the dendritic deposits.

IL electrolytes can play an important role in the construction of high performance AAEM supercapatteries. Creating economical, functional, and stable IL electrolytes is not a trivial task, but it is worthy of more effort and attempts, since the physical and chemical properties of ILs are largely tuneable by a judicious combination of cations and anions. Notably, appropriate additives can be rationally selected or designed to improve the drawbacks of ILs (e.g., low ionic conductivity). Meanwhile, film-forming properties such as SEI on AAEMs, corrosion toward current collector/AAEMs, and structure matching with the positrode should also be carefully considered.

The SEI with electron passivation and Li^+ ion conduction is a fortunate compromise between highly reactive AAEMs negatodes and relatively unstable electrolytes in LIBs. However, such SEIs from LIBs are hard to mimic in other EESDs. For example, the SEI is often absent on Mg negatodes. Theoretically, nearly 100% CE renders exceptional electrochemical properties for Mg without the SEI. Furthermore, many tricky problems that are related to SEI formation such as the electrolyte drying out, SEI-induced deviation in spatial charge, and metal negatode consumption may not be present in other multivalent metal batteries. Last but not least, faster dis-/charging processes may be easily achieved owing to barrier-free in the absence of SEI. For example, aluminium (Al)-chalcogen battery may achieve SEI-free on Al metal using molten-salt electrolyte composed of NaCl-KCl-AlCl_3 and show excellent capacity retention at the ultrahigh current rate (200C).¹⁴⁸

In current views, the key technological point for AAEM metal and ion EESDs lies in whether or not the electrolyte decomposition can form a uniform SEI layer that conducts the respective AAEM ions. However, if there is the possibility of developing an SEI-free metal negatode from an IL electrolyte with high positrode stability, it will be much more attractive for achieving highly stable and efficient electrochemical performances (e.g., higher CE). This strong anti-reduction nature of the cation and anion from ILs and AAEMs is expected. Meanwhile, other challenges of ILs e.g., poor

negatrode stability and high cost or corrosion toward the current collector, are not expected to be evident. Alternatively, developing AAEM ion conducting interphases could be the most viable choice to facilitate similar high cycle durability of commercial LIBs for AAEMs supercapatteries.

2.2.2. High temperature potentials

From the analyses and discussions above, it is clear that IL-AAEMs supercapatteries have three common key aspects for future improvements, namely low ionic conductivity, dendritic deposition and SEI formation. In addition to the above discussed approaches, an alternative is to prepare the electrolyte with molten salts which are the high temperature counterparts of ionic liquids. Because of their high working temperatures, molten salts are water-like liquid in terms of viscosity. For example, the viscosity of water is about 1.0 mPa s at room temperature, whilst molten alkali chlorides show very comparable viscosities at temperatures 50 °C above their melting points.¹⁴⁹ For a general comparison, the viscosity ranges from 400 mPa s to 1200 mPa s for ionic liquids of alkyl-substituted ammonium cations with different anions.⁸⁴ Another beneficial coincidence is that AAEMs have usually lower melting temperatures than, e.g., their chloride salts, which means these metals can be in **the** liquid state at the working temperatures of molten salts. Consequently, deposition occurs on the liquid negatrode, avoiding any formation of dendrites. The most important difference is perhaps that no SEI is needed to protect the AAEM negatropes from reactions with the molten salts.

However, to our best knowledge, there is not yet any purposely reported study on molten salt supercapatteries, although a noticeable portion of the literature is on high temperature rechargeable batteries of which AAEMs were used to make the negatrode. In more recent years, molten salt supercapacitors are emerging. Therefore, it is not unreasonable to postulate molten salt supercapatteries as a concept and explore their positive and challenging prospects.

The effort in history to utilise molten salts for EESDs **was** on batteries in which the

dominant charge storage follows the Nernstian mechanism. Molten salt batteries have regained significant attention in recent years due to their high specific energy, long cycle life, and ability to operate at high temperatures. It is interesting to note that in conventional high power batteries with organic electrolytes such as LIBs, heat build-up inside the batteries during dis-/charging is a technical and safety challenge and must be dissipated effectively and quickly. Consequently, sophisticated heat management is needed in terms of design, manufacture and material selection, increasing further the cost. However, for molten salt EESDs which are especially suitable for high power applications, there is no need for heat management because the Joule heat resulting from current passing through the electrode and electrolyte is needed to maintain the working temperature.

One nontrivial component of molten salt batteries is the negatode material. Compared to other materials, metal negatode reveals numerous advantages as discussed before, including high theoretical specific capacity, very negative electrode potentials, high electronic conductivities and considerable compatibility with molten salt electrolyte and metal-free positrodes (e.g., O₂).¹⁵⁰ As in room temperature electrolytes, metallic negatodes, such as Li, Na, Mg, Al and Fe, have been investigated extensively in molten salt batteries.¹⁵¹⁻¹⁶² For instance, Giordani et al.¹⁵² reported a Li-O₂ battery with 95% energy efficiency achieved in molten LiNO₃-KNO₃ eutectic at 150 °C. However, the cycling stability was poor (<50 cycles, 2.6 mAh cm⁻² at 0.6 mA cm⁻²), due to the oxidation of carbon and consequent formation of Li₂CO₃ at the positrode.

Xie et al.¹⁵³ also studied the Li-O₂ battery in the molten eutectic mixture of LiNO₃-KNO₃ with a nanostructured Ni/LiNO₃-KNO₃ composite positrode in which a thin layer of Li_xNiO₂ was formed in situ on individual Ni nanoparticles and functioned as the catalyst for O-O bond cleavage and formation. A columbic efficiency of ~100% was achieved, also at 150 °C, with promising stability (150 cycles, 0.5 mAh cm⁻² at 0.2 mA cm⁻²). It should be noted that this work was focused on the O₂ positrode improvement, mentioning little about the performance of the Li negatode. Since the testing temperature was 150 °C, the Li negatode, a disk, was in a solid state and prone to

dendritic deposition. Although this was not mentioned, the Li negatrodde was separated from the molten salt by a solid electrolyte, $\text{Li}_{1.5}\text{Al}_{0.5}\text{Ge}_{1.5}(\text{PO}_4)_3$ (LAGP), which obviously helped to mitigate the impact of dendritic deposition. Further, the LAGP functioned as a barrier preventing any product from the positrodde to reach the Li negatrodde, enhancing the coulombic efficiency of the cell.

Yin et al.¹⁵⁴ investigated the liquid metal battery using a liquid Li-Pb alloy negatrodde and a liquid Pb positrodde in molten LiCl-KCl containing PbCl_2 . With a porous TiN membrane, the cell achieved a coulombic efficiency of 92% with a round-trip energy efficiency of 71% at 150 mA cm^{-2} at $410 \text{ }^\circ\text{C}$. The very unusual and novel feature of this work is the use of an electron conducting TiN membrane. In conventional EESDs, a porous and/or ion conducting membrane is used to physically separate and electronically insulate the positrodde from the negatrodde. In terms of function, this membrane forms a part of the electrolyte. On the contrary, in the work of Yin et al., the TiN membrane was actually used to hold the liquid Li-Pb negatrodde above the liquid Pb positrodde. It is therefore a separator for physical prevention of the direct contact and mixing between the two liquid metal electrodes, but the electronic insulation between positrodde and negatrodde was achieved by a layer of molten salt. Therefore, the TiN membrane formed a part of the negatrodde, instead of the electrolyte. In principle, this (-) Pb-Li || Pb (+) cell should involve only the reversible conversion between Pb (0) and Pb (II) alternately on positrodde and negatrodde. In the liquid Pb-Li negatrodde, Li functioned as a solvent to lower the activity of Pb (0). However, because of the presence of Li^+ in the molten salt electrolyte, the occurrence of the conversion between Li (0) and Li (I) may not be excluded completely.

Nevertheless, the relatively high cost of lithium because of the limited earth crust abundance could be a major problem inhibiting its wide usage. A viable alternative is sodium negatrodde which costs less and is far more abundant on the earth. One attractive example for both transportation and stationery applications is the sodium-metal halide (Na-MH or ZEBRA) battery using a solid membrane of Na^+ ion conductor, i.e. Na- β -alumina as the primary electrolyte and molten sodium tetrachloroaluminate (NaAlCl_4) as the secondary electrolyte, which has been produced commercially by the

FzSoNick Group. Relatively high specific energy (120 Wh kg^{-1}) can be achieved at $300 \text{ }^\circ\text{C}$ with energy efficiency varying from 90-95%.¹⁶³ Besides, Shamin et al.¹⁵⁶ reported a 90% energy efficiency at $265 \text{ }^\circ\text{C}$ for a ZEBRA battery module (48TL200) from FzSoNick with promising stability (a degradation rate of 0.0046%/cycle over 150 cycles). In 2022, Zhu et al.¹⁵⁷ reported, as shown in Fig. 11a, $\beta\text{-Al}_2\text{O}_3$ membrane enabled Na-O₂ battery in molten $\text{NaNO}_3\text{-KNO}_3\text{-CsNO}_3$ eutectic at $270 \text{ }^\circ\text{C}$ with considerable areal energy and power (33 mWh cm^{-2} and 19 mW cm^{-2} , respectively). The work also revealed dynamic and kinetic complications around the oxygen positrode and the $\beta\text{-Al}_2\text{O}_3$ membrane, restricting the battery from deep discharging and high power operation. Nonetheless, no issue was mentioned on the liquid Na negatrode.

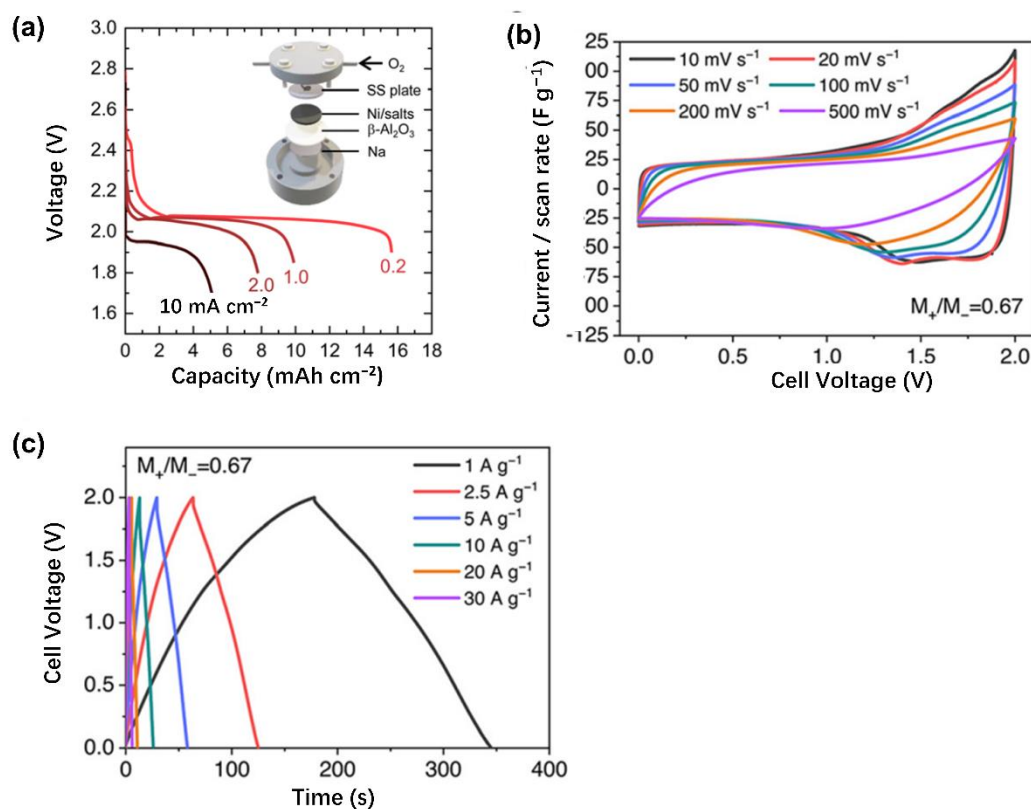


Figure 11. (a) Discharge curves of at indicated current densities of a laboratory molten-salt Na-O₂ battery as schematically illustrated with a liquid Na negatrode, a two-phase electrolyte of $\beta\text{-Al}_2\text{O}_3$ membrane plus molten mixture of $\text{NaNO}_3\text{-KNO}_3\text{-CsNO}_3$, and a sintered Ni powder positrode attached to a stainless steel (SS) mesh, current collector, through which the inlet and outlet of O₂ gas occur. (b) CVs and (c) GCDs at indicated

potential scan rates and specific currents, respectively, of an asymmetrical cell of carbon positrode and negatrode at the mass ratio of $M_+/M_- = 0.67$ in molten $\text{AlCl}_3\text{-LiCl-KCl}$ (molar ratio = 0.6:0.2:0.2) at 125 °C. (Adapted with permission from ref. [157] and ref. [164], Copyright 2022, Royal Society of Chemistry).

Molten salt batteries utilising other earth abundant metals as negatodes (e.g., Mg, Ca, Al and Fe) have also been reported in $\text{MgCl}_2\text{-KCl-NaCl}$ ¹⁵⁸, LiCl-NaCl-CaCl_2 ¹⁵⁹, $\text{AlCl}_3\text{-NaCl-LiCl-KCl}$ ¹⁶⁰ and $\text{Fe}_3\text{O}_4\text{-Na}_2\text{CO}_3\text{-K}_2\text{CO}_3$ ¹⁶² with remarkable efficiency and life span. It is worth noting that a strong competitor to AAEMs is Al which has also been researched due to the large theoretical specific charge capacity/charge density caused by three-electrons transfer in one redox couple (Al^{3+}/Al). Song et al.¹⁶⁰ developed an Al-ion battery in molten NaAlCl_4 with a coulombic efficiency higher than 99% at 120 °C. An extremely long cycling life (up to 9000 cycles) was also achieved at a 4000 mA g^{-1} . Furthermore, $\text{AlCl}_3\text{-NaCl-LiCl-KCl}$ was utilised by Tu et al. for lowering the working temperature of Al-ion battery.¹⁶¹ A columbic efficiency of 91.3% was obtained with a specific capacity of 114.9 mAh g^{-1} at 90 °C over 1500 cycles.

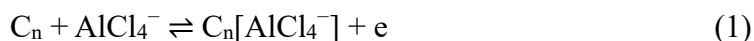
These few selected studies on molten salt batteries are by no means exhaustive of the literature, but they have already provided valuable insights into the electrochemical performance of these molten salts to accommodate reversible and stable dis-/charging of AAEM and other metal negatodes. It is particularly worth mentioning that these studies have never encountered problems from dendrite and/or SEI formation, pronouncing a clear advantage of molten salts over both organic and IL electrolytes. However, the positrode design and material selection for Nernstian storage remain a case by case challenge to molten salt batteries, leaving an opportunity for the development of capacitive positrodes and molten salt supercapattery.

In more recent efforts to develop molten salt EESDs, apart from rechargeable batteries, supercapacitors have emerged, owing to their unmatched power capability and cycle life proven in aqueous and organic electrolytes at room temperature. In comparison with their aqueous or organic counterparts, inorganic molten salt electrolytes offer a complementary choice with wide electrochemical stability windows

(ESWs) comparable with those of organic electrolytes, high ionic conductivity and low material cost, matching those of aqueous electrolytes.¹⁶⁵ Whilst it is possible to use molten salt EESDs in an ambient environment, their high temperature applications are unmatched by their counterparts with aqueous and organic electrolytes.

The first supercapacitor with an inorganic molten salt electrolyte was perhaps reported in 2013.¹⁶⁶ The eutectic mixture of LiNO₃, NaNO₃ and CsNO₃ was used as the electrolyte in a symmetrical supercapacitor of activated carbon (1700 m² g⁻¹ in specific surface area). Capacitive storage was investigated by CV at 140 °C, exhibiting a satisfactory rectangular feature without any current peaks. The specific cell capacitance was measured to reach 31.5 F g⁻¹ which is comparable to that of an aqueous supercapacitor. The work revealed mismatching wetting between the molten salt and activated carbon and offered a simple solution by pre-soaking the activated carbon in the aqueous solution of 0.1 M NaNO₃ followed by drying before use in the molten salt. The cell worked to a maximum cell voltage of 1.6 V, giving rise to a specific energy of 22.8 Wh kg⁻¹.

A significant improvement was reported by Wang et al.¹⁶⁴, employing activated carbon electrodes in molten AlCl₃-NaCl-LiCl to form a supercapacitor which exhibited a fairly high specific energy (50.4 Wh kg⁻¹) at 125 °C and a specific power of 1.1 kW kg⁻¹. The achieved high cycling stability (99.8% capacitance retention after 10,000 cycles) revealed the feasibility of molten salt supercapacitors. Specifically, the enhanced storage capacity was attributed mainly to the intercalation of the AlCl₄⁻ anion into the carbon via the reaction (1) below.



The electrode potential of reaction (1) is highly anodic, which means that at high cell voltages, the forward process of reaction (1) should occur on the carbon positrode, but the reverse on the carbon negatrode. This feature is reflected by CVs at higher cell voltages showing increased discharging and charging currents with small peaks, and by GCDs exhibiting smaller gradients (dV/dt) as shown in Fig. 11b-c. Because reaction (1) and its CV and GCD features are indicative of the presence of the Faradaic or Nernstian storage mechanism, the cell was actually a supercapattery.

In the same study¹⁶⁴, other types of molten salt consisting of redox active chloro-aluminate ions, bromine ions, and iodine ions were also examined with a promising specific capacitance (268 to 379 F g⁻¹). These values are comparable to those of non-aqueous supercapacitors, promising the employment of molten salt in supercapacitors for various high-temperature applications.

Unfortunately, the familiar respective drawbacks of supercapacitors (small energy capacity) and rechargeable batteries (low power capability) shown at room temperature also appear at high temperatures. It is therefore natural to consider the prospects of molten salt supercapatteries, although there is a paucity of research in this direction, except for the unnoticed finding in the work of Wang et al.¹⁶⁴ Experiences and skills can be learnt from research on batteries and supercapacitors with ionic liquids or molten salts as the electrolyte. For example, based on the past studies in refs.¹⁵⁵ to ¹⁵⁷ on liquid Na negatrotrode and refs.¹⁶⁶ and ¹⁶⁴ on activated carbon positrode, it can be anticipated that the first molten salt supercapattery can be made from coupling these two electrodes in a variety of inorganic molten salts with or even without using a Na⁺ ion conducting ceramic membrane. Introducing redox additives in the molten salts should also be considered to enhance the charge capacity of the capacitive positrode.¹⁵⁶

It is worth mentioning that because molten salts freeze at room temperatures, a fully charged molten salt EESD can be kept on a shelf for a long period until the next designated time of discharge without suffering from any self-discharge. This is because the solidified salt is an insulator to both electrons and ions. This storage advantage is unmatched by other electrolyte based EESDs in which self-discharge is inevitable, particularly supercapacitors. A storage life over a year or longer is needed in many remote areas such as in the south and north poles and on the Moon or Mars. Of course, to bring the solidified salts back to the working temperature would require pre-heating. This can be achieved by, for example, using the so called thermite (thermate) that is a composite of metal fuel and oxidant and can, upon ignition, undergo highly exothermic but non-explosive redox reaction for fast heating in confined areas.¹⁶⁷

Further, molten salts supercapatteries are suitable for both low and high temperature applications, but it is their high temperature uses that make them unique EESDs for unusual applications in, for example, concentrated solar power (CSP) plants in which molten salts are used for thermal energy transfer and storage. Apparently, with molten salts EESDs, the CSP plant can engage in direct electricity storage, taking advantage of the sunlight heated high temperature molten salts. Particularly, with their expected relatively low cost, capability of high energy and power density storage, and durable services, molten salts supercapatteries could be an ideal choice to help the CPS plant to achieve storage of both heat and electricity.

Like other emerging technologies, molten salt AAEM supercapatteries also have technical challenges. The most common one is the supporting materials for making the molten salt container. In the authors' experience, molten salts themselves are **non-corrosive** to metals, but can become aggressive in the presence **of** moisture and/or oxygen. Therefore, drying the salt before melting and sealing the EESD completely from air are crucial to **maintaining** stability and durability. On the other hand, very little is known about the transferability of various existing room temperature supercapacitor positive for molten salts. Last but not the list, cell design and material selection are very important to accommodate the **high** temperature liquid salt without any internal and external leak so that it is easy and safe to position the EESD in any orientation.

Conclusion

In summary, supercapatteries combining a supercapacitor positive with an AAEM negative of high theoretical charge capacity and most negative potentials with optimised IL electrolytes are a promising strategy to approach the next generation high performance EESDs. Although various studies on **IL-based** electrolytes for supercapacitors and **AAEM-based** batteries are widely reported, research related to IL-AAEM supercapatteries is still climbing a long and steep hill. There are challenges from unfavourable IL properties such as low conductivity, possible leakage risk, high

selectivity to material structure/composition, strong corrosivity, and poor functionality. These drawbacks of ILs are twinned with challenges from using AAEM negatropes such as SEI formation, electrolyte depletion, and polymorphous metal deposit. Also, the relevant mechanism of **combining** capacitive and Nernstian charge storage still needs further detailed study. Particularly, innovative synthesis of low cost, functional, and stable IL electrolytes to solve both the issues of IL electrolytes and AAEM negatropes is worth putting the greatest effort. As it says, “there are always more ways than difficulties” for supercapattery development to serve our future energy needs. Along this line, we propose to utilise molten salts, the high temperature counterpart of ILs, in EESDs, particularly AAEM supercapatteries in search for solutions to almost all kinetic, dynamic and mechanistic difficulties encountered in IL and organic electrolytes, in combination with careful and innovative designs in materials selection and processing and cell manufacture.

Acknowledgments

We would like to thank current and past financial supports from the CSC (File No. 202108330377, Q.G), DTP Programme of the UNNC and NIMTE, CAS (2019 -2023, Q.G.), student families (P.Y.F. and Y.H.Z.), Innovate UK (Smart Grants, 10017140), Daphne Jackson Fellowship (2020-2022, L.G.), Propulsion Futures Beacon of Excellence of the UoN (2021-2022), Municipal Bureau of Science and Technology (3315 Plan and 2014A35001-1), E.ON AG (Energy Storage Award 2007), Royal Society (Braine Mercer Feasibility Award, 2006), Leverhulme Trust (A.K.C.) and EPSRC (EP/J000582/1, GR/R68078).

Conflicts of interest

There are no conflicts of interest to declare.

References

1. F. Yu, C. Zhang, F. Wang, Y. Gu, P. Zhang, E. R. Waclawik, A. Du, K. Ostrikov and H. Wang, *Materials Horizons*, 2020, **7**, 495-503.
2. W. Liu, P. Oh, X. Liu, M. J. Lee, W. Cho, S. Chae, Y. Kim and J. Cho, *Angew Chem Int Ed Engl*, 2015, **54**, 4440-4457.
3. J. Hu, W. Huang, L. Yang and F. Pan, *Nanoscale*, 2020, **12**, 15036-15044.
4. G. Z. Chen, *International Materials Reviews*, 2016, **62**, 173-202.
5. L. Yu and G. Z. Chen, *Faraday Discuss*, 2016, **190**, 231-240.
6. L. Yu and G. Z. Chen, *Front Chem*, 2019, **7**, 272.
7. H. Sakaebe and H. Matsumoto, *Electrochemistry Communications*, 2003, **5**, 594-598.
8. L. Guan, G. Z. Chen, A. K. Croft and D. M. Grant, *Journal of The Electrochemical Society*, 2022, **169**, 030529.
9. Q. Guo, W. Deng, S. Xia, Z. Zhang, F. Zhao, B. Hu, S. Zhang, X. Zhou, G. Z. Chen and Z. Liu, *Nano Research*, 2021, **14**, 3585-3597.
10. Q. Guo, Y. Yu, S. Xia, C. Shen, D. Hu, W. Deng, D. Dong, X. Zhou, G. Z. Chen and Z. Liu, *ACS Applied Materials & Interfaces*, 2022, **14**, 46043-46055.
11. Q. Guo, S. Wang, Y. Li, J. Wang, Y. Wu, Y. Yu, S. Xia, D. Hu, B. Hu, Z. Ye, X. Zhou, G. Z. Chen and Z. Liu, *Journal of Power Sources*, 2023, **580**, 233401.
12. S. A. Ferdousi, L. A. O'Dell, J. Sun, Y. Hora, M. Forsyth and P. C. Howlett, *ACS Appl Mater Interfaces*, 2022, **14**, 15784-15798.
13. H. Wang, X. Feng, Y. Chen, Y.-S. Liu, K. S. Han, M. Zhou, M. H. Engelhard, V. Murugesan, R. S. Assary, T. L. Liu, W. Henderson, Z. Nie, M. Gu, J. Xiao, C. Wang, K. Persson, D. Mei, J.-G. Zhang, K. T. Mueller, J. Guo, K. Zavadil, Y. Shao and J. Liu, *ACS Energy Letters*, 2019, **5**, 200-206.
14. H. Sun, G. Zhu, Y. Zhu, M. C. Lin, H. Chen, Y. Y. Li, W. H. Hung, B. Zhou, X. Wang, Y. Bai, M. Gu, C. L. Huang, H. C. Tai, X. Xu, M. Angell, J. J. Shyue and H. Dai, *Adv Mater*, 2020, **32**, e2001741.

15. S. Azmi, M. F. Koudahi and E. Frackowiak, *Energy & Environmental Science*, 2022, **15**, 1156-1171.
16. J. Wu, Q. Liang, X. Yu, Q.-F. Lü, L. Ma, X. Qin, G. Chen and B. Li, *Advanced Functional Materials*, 2021, **31**, 2011102.
17. M. Durth, C. Prieto, A. Rodríguez-Sánchez, D. Patiño-Rodríguez and L. F. Cabeza, *Solar Energy*, 2019, **182**, 57-63.
18. R. Benages-Vilau, T. Calvet, M. A. Cuevas-Diarte and H. A. J. Oonk, *Phase Transitions*, 2016, **89**, 1-20.
19. B. D'Aguanno, M. Karthik, A. N. Grace and A. Floris, *Scientific Reports*, 2018, **8**, 10485.
20. T. van Ree, *Current Opinion in Electrochemistry*, 2020, **21**, 22-30.
21. W. Li, J. R. Dahn and D. S. Wainwright, *Science*, 1994, **264**, 1115-1118.
22. Y. Yamada, K. Usui, K. Sodeyama, S. Ko, Y. Tateyama and A. Yamada, *Nature Energy*, 2016, **1**, 16129.
23. E. Adelowo, A. R. Baboukani, O. Okpowe, I. Khakpour, M. Safa, C. Chen and C. Wang, *Journal of Power Sources*, 2020, **455**, 227987.
24. S. Kaipannan and S. Marappan, *Scientific Reports*, 2019, **9**, 1104.
25. Q. Gao, *Journal of Energy Chemistry*, 2019, **38**, 219-224.
26. J. B. Goodenough and Y. Kim, *Chemistry of materials*, 2010, **22**, 587-603.
27. K. C. Lethesh, A. Bahaa, M. Abdullah, M. O. Bamgbopa and R. A. Susantyoko, *Frontiers in Chemistry*, 2022, **10**, 859304.
28. L. Miao, Z. Song, D. Zhu, L. Li, L. Gan and M. Liu, *Energy & Fuels*, 2021, **35**, 8443-8455.
29. J. Feng, Y. Wang, Y. Xu, Y. Sun, Y. Tang and X. Yan, *Energy & Environmental Science*, 2021, **14**, 2859-2882.
30. S. Pan, M. Yao, J. Zhang, B. Li, C. Xing, X. Song, P. Su and H. Zhang, *Frontiers in Chemistry*, 2020, **8**, 261.
31. A. Guerfi, M. Dontigny, P. Charest, M. Petitclerc, M. Lagacé, A. Vijn and K. Zaghbi, *Journal of Power Sources*, 2010, **195**, 845-852.
32. S. Fleischmann, M. Widmaier, A. Schreiber, H. Shim, F. M. Stiemke, T. J.

- Schubert and V. Presser, *Energy Storage Materials*, 2019, **16**, 391-399.
33. P. Navalpotro, J. Palma, M. Anderson and R. Marcilla, *Journal of Power Sources*, 2016, **306**, 711-717.
34. I. Plitz, A. DuPasquier, F. Badway, J. Gural, N. Pereira, A. Gmitter and G. Amatucci, *Applied Physics A*, 2006, **82**, 615-626.
35. H. A. Andreas, *Journal of The Electrochemical Society*, 2015, **162**, A5047.
36. G. G. Amatucci, F. Badway, A. Du Pasquier and T. Zheng, *Journal of the Electrochemical Society*, 2001, **148**, A930.
37. A. Yoshino, *Angewandte Chemie International Edition*, 2012, **51**, 5798-5800.
38. F. Zhang, T. Zhang, X. Yang, L. Zhang, K. Leng, Y. Huang and Y. Chen, *Energy & Environmental Science*, 2013, **6**, 1623-1632.
39. E. Lim, H. Kim, C. Jo, J. Chun, K. Ku, S. Kim, H. I. Lee, I.-S. Nam, S. Yoon and K. Kang, *ACS nano*, 2014, **8**, 8968-8978.
40. H. Wang, Z. Xu, Z. Li, K. Cui, J. Ding, A. Kohandehghan, X. Tan, B. Zahiri, B. C. Olsen and C. M. Holt, *Nano letters*, 2014, **14**, 1987-1994.
41. Y.-g. Wang, J.-y. Luo, C.-x. Wang and Y.-y. Xia, *Journal of the Electrochemical Society*, 2006, **153**, A1425.
42. J.-M. Tarascon and M. Armand, *nature*, 2001, **414**, 359-367.
43. D. Lin, Y. Liu and Y. Cui, *Nature nanotechnology*, 2017, **12**, 194-206.
44. Q. Zhong, B. Liu, B. Yang, Y. Li, J. Li and X. Yan, *Chinese Chemical Letters*, 2021, **32**, 3496-3500.
45. B. Liu, J. Chen, B. Yang, Z. Lin, C. J. Zhang, Z. Zeng, M. Jiao, L. Liu, Y. Sun and R. Hou, *Energy Storage Materials*, 2021, **42**, 154-163.
46. T. C. Mendes, F. Zhou, A. J. Barlow, M. Forsyth, P. C. Howlett and D. R. MacFarlane, *Sustainable Energy & Fuels*, 2018, **2**, 763-771.
47. G. A. dos Santos Junior, V. D. Fortunato, G. G. Silva, P. F. Ortega and R. L. Lavall, *Electrochimica Acta*, 2019, **325**, 134900.
48. G. A. dos Santos Junior, V. D. Fortunato, G. A. Bastos, G. G. Silva, P. F. Ortega and R. L. Lavall, *ACS Applied Energy Materials*, 2020, **3**, 9028-9039.
49. Y. S. Yun, J. H. Kim, S.-Y. Lee, E.-G. Shim and D.-W. Kim, *Journal of Power*

- Sources*, 2011, **196**, 6750-6755.
50. N. Hirota, K. Okuno, M. Majima, A. Hosoe, S. Uchida and M. Ishikawa, *Electrochimica Acta*, 2018, **276**, 125-133.
 51. H. Sun, P. Liang, G. Zhu, W. H. Hung, Y.-Y. Li, H.-C. Tai, C.-L. Huang, J. Li, Y. Meng, M. Angell, C.-A. Wang and H. Dai, *Proceedings of the National Academy of Sciences*, 2020, **117**, 27847-27853.
 52. P. Meister, V. Küpers, M. Kolek, J. Kasnatscheew, S. Pohlmann, M. Winter and T. Placke, *Batteries & Supercaps*, 2021, **4**, 504-512.
 53. S. Chen, C. Niu, H. Lee, Q. Li, L. Yu, W. Xu, J.-G. Zhang, E. J. Dufek, M. S. Whittingham, S. Meng, J. Xiao and J. Liu, *Joule*, 2019, **3**, 1094-1105.
 54. M. S. Park, S. B. Ma, D. J. Lee, D. Im, S.-G. Doo and O. Yamamoto, *Scientific reports*, 2014, **4**, 3815.
 55. S. W. Kim, D. H. Seo, X. Ma, G. Ceder and K. Kang, *Advanced Energy Materials*, 2012, **2**, 710-721.
 56. G. H. Newman and L. P. Klemann, *Journal of The Electrochemical Society*, 1980, **127**, 2097.
 57. K. West, B. Zachau-Christiansen, T. Jacobsen and S. Skaarup, *Journal of Power Sources*, 1989, **26**, 341-345.
 58. J. M. Tarascon and G. W. Hull, *Solid State Ionics*, 1986, **22**, 85-96.
 59. D. Stevens and J. Dahn, *Journal of the Electrochemical Society*, 2000, **147**, 1271.
 60. K. Lu, B. Song, X. Gao, H. Dai, J. Zhang and H. Ma, *Journal of Power Sources*, 2016, **303**, 347-353.
 61. C. Zhao, L. Liu, X. Qi, Y. Lu, F. Wu, J. Zhao, Y. Yu, Y.-S. Hu and L. Chen, *Advanced Energy Materials*, 2018, **8**, 1703012.
 62. H. W. Kwak, M. E. Lee, H.-J. Jin and Y. S. Yun, *Journal of Power Sources*, 2019, **418**, 218-224.
 63. S. Park, J. C. Hyun, J. H. Kwak, M. E. Lee, H.-J. Jin and Y. S. Yun, *Applied Surface Science*, 2020, **513**, 145848.
 64. D. Iermakova, R. Dugas, M. Palacín and A. Ponrouch, *Journal of The Electrochemical Society*, 2015, **162**, A7060.

65. W. Zhou, Y. Li, S. Xin and J. B. Goodenough, *ACS central science*, 2017, **3**, 52-57.
66. R. Wibowo, L. Aldous, E. I. Rogers, S. E. Ward Jones and R. G. Compton, *The Journal of Physical Chemistry C*, 2010, **114**, 3618-3626.
67. H. D. Yoo, I. Shterenberg, Y. Gofer, R. E. Doe, C. C. Fischer, G. Ceder and D. Aurbach, *Journal of The Electrochemical Society*, 2014, **161**, A410.
68. Z. Lu, A. Schechter, M. Moshkovich and D. Aurbach, *Journal of Electroanalytical Chemistry*, 1999, **466**, 203-217.
69. H. Dong, O. Tutusaus, Y. Liang, Y. Zhang, Z. Lebens-Higgins, W. Yang, R. Mohtadi and Y. Yao, *Nature Energy*, 2020, **5**, 1043-1050.
70. S. Hou, X. Ji, K. Gaskell, P.-f. Wang, L. Wang, J. Xu, R. Sun, O. Borodin and C. Wang, *Science*, 2021, **374**, 172-178.
71. H. Chu, Z. Zhang, Z. Song, A. Du, S. Dong, G. Li and G. Cui, *Chemical Communications*, 2021, **57**, 9430-9433.
72. W. Zuo, R. Li, C. Zhou, Y. Li, J. Xia and J. Liu, *Advanced science*, 2017, **4**, 1600539.
73. X. Deng, L. Li, G. Zhang, X. Zhao, J. Hao, C. Han and B. Li, *Energy Storage Materials*, 2022, **53**, 467-481.
74. P. Hundekar, S. Basu, X. Fan, L. Li, A. Yoshimura, T. Gupta, V. Sarbada, A. Lakhnot, R. Jain and S. Narayanan, *Proceedings of the National Academy of Sciences*, 2020, **117**, 5588-5594.
75. L. Qin, Y. Lei, H. Wang, J. Dong, Y. Wu, D. Zhai, F. Kang, Y. Tao and Q. H. Yang, *Advanced Energy Materials*, 2019, **9**, 1901427.
76. K. Yoshii, T. Masese, M. Kato, K. Kubota, H. Senoh and M. Shikano, *ChemElectroChem*, 2019, **6**, 3901-3910.
77. H. Yamamoto, C.-Y. Chen, K. Kubota, K. Matsumoto and R. Hagiwara, *The Journal of Physical Chemistry B*, 2020, **124**, 6341-6347.
78. Y. Wuhai, Z. Jingwen, W. Cunguo and C. Guanglei, *Energy Storage Science and Technology*, 2019, **8**, 26.
79. H. Park, C. J. Bartel, G. Ceder and P. Zapol, *Advanced Energy Materials*, 2021,

- 11, 2101698.
80. X. Gao, X. Liu, A. Mariani, G. A. Elia, M. Lechner, C. Streb and S. Passerini, *Energy & Environmental Science*, 2020, **13**, 2559-2569.
81. N. Wu, W. Yao, X. Song, G. Zhang, B. Chen, J. Yang and Y. Tang, *Advanced Energy Materials*, 2019, **9**, 1803865.
82. T. Stettner, R. Dugas, A. Ponrouch and A. Balducci, *Journal of The Electrochemical Society*, 2020, **167**, 100544.
83. G. A. Giffin, *Journal of Materials Chemistry A*, 2016, **4**, 13378-13389.
84. F. Philippi and T. Welton, *Physical Chemistry Chemical Physics*, 2021, **23**, 6993-7021.
85. D. Rauber, F. Philippi, B. Kuttich, J. Becker, T. Kraus, P. Hunt, T. Welton, R. Hempelmann and C. W. M. Kay, *Physical Chemistry Chemical Physics*, 2021, **23**, 21042-21064.
86. S. Tang, G. A. Baker and H. Zhao, *Chemical Society Reviews*, 2012, **41**, 4030-4066.
87. B. S. Lalia, N. Yoshimoto, M. Egashira and M. Morita, *Journal of Power Sources*, 2010, **195**, 7426-7431.
88. N. Chen, Y. Guan, J. Shen, C. Guo, W. Qu, Y. Li, F. Wu and R. Chen, *ACS Appl Mater Interfaces*, 2019, **11**, 12154-12160.
89. B. Rupp, M. Schmuck, A. Balducci, M. Winter and W. Kern, *European Polymer Journal*, 2008, **44**, 2986-2990.
90. R. L. Lavall, S. Ferrari, C. Tomasi, M. Marzantowicz, E. Quartarone, A. Magistris, P. Mustarelli, S. Lazzaroni and M. Fagnoni, *Journal of Power Sources*, 2010, **195**, 5761-5767.
91. S. Shiraishi, N. Nishina, A. Oya and R. Hagiwara, *Electrochemistry*, 2005, **73**, 593-596.
92. B. Akinwolemiwa, C. Peng and G. Z. Chen, *Journal of The Electrochemical Society*, 2015, **162**, A5054-A5059.
93. N. Jayaprakash, S. K. Das and L. A. Archer, *Chemical Communications*, 2011, **47**, 12610-12612.

94. L. D. Reed and E. Menke, *Journal of The Electrochemical Society*, 2013, **160**, A915.
95. J. Muldoon, C. B. Bucur, A. G. Oliver, J. Zajicek, G. D. Allred and W. C. Boggess, *Energy Environ. Sci.*, 2013, **6**, 482-487.
96. L. Zhang, S. Yang, J. Chang, D. Zhao, J. Wang, C. Yang and B. Cao, *Frontiers in Chemistry*, 2020, **8**, 413.
97. H. Yu, J. Wu, L. Fan, K. Xu, X. Zhong, Y. Lin and J. Lin, *Electrochimica Acta*, 2011, **56**, 6881-6886.
98. H. Yu, J. Wu, L. Fan, Y. Lin, K. Xu, Z. Tang, C. Cheng, S. Tang, J. Lin, M. Huang and Z. Lan, *Journal of Power Sources*, 2012, **198**, 402-407.
99. J. Jang, J. S. Shin, S. Ko, H. Park, W. J. Song, C. B. Park and J. Kang, *Advanced Energy Materials*, 2022, **12**, 2103955.
100. M. Y. Yang, S. V. Zybin, T. Das, B. V. Merinov, W. A. Goddard, E. K. Mok, H. J. Hah, H. E. Han, Y. C. Choi and S. H. Kim, *Advanced Energy Materials*, 2022, **13**, 2202949.
101. U. Pal, D. Rakov, B. Lu, B. Sayahpour, F. Chen, B. Roy, D. R. MacFarlane, M. Armand, P. C. Howlett, Y. S. Meng and M. Forsyth, *Energy & Environmental Science*, 2022, **15**, 1907-1919.
102. N. W. Li, Y. X. Yin, J. Y. Li, C. H. Zhang and Y. G. Guo, *Adv Sci (Weinh)*, 2017, **4**, 1600400.
103. G. N. Lewis and F. G. Keyes, *Journal of the American Chemical Society*, 1913, **35**, 340-344.
104. J. B. Goodenough and H. Gao, *Science China Chemistry*, 2019, **62**, 1555-1556.
105. H. Wang, C. Zhu, D. Chao, Q. Yan and H. J. Fan, *Advanced Materials*, 2017, **29**, 1702093.
106. J. Ding, W. Hu, E. Paek and D. Mitlin, *Chemical Reviews*, 2018, **118**, 6457-6498.
107. X. Gao, H. Wu, C. Su, C. Lu, Y. Dai, S. Zhao, X. Hu, F. Zhao, W. Zhang, I. P. Parkin, C. J. Carmalt and G. He, *Energy & Environmental Science*, 2023, **16**, 1364-1383.

108. A. Ponrouch, J. Bitenc, R. Dominko, N. Lindahl, P. Johansson and M. R. Palacin, *Energy Storage Materials*, 2019, **20**, 253-262.
109. M. Li, J. Lu, X. Ji, Y. Li, Y. Shao, Z. Chen, C. Zhong and K. Amine, *Nature Reviews Materials*, 2020, **5**, 276-294.
110. D. Fouchard and J. B. Taylor, *Journal of Power Sources*, 1987, **21**, 195-205.
111. N. S. Gingrich and L. Heaton, *The Journal of Chemical Physics*, 1961, **34**, 873-878.
112. S. Jiao, J. Zheng, Q. Li, X. Li, M. H. Engelhard, R. Cao, J.-G. Zhang and W. Xu, *Joule*, 2018, **2**, 110-124.
113. P. Verma, P. Maire and P. Novák, *Electrochimica Acta*, 2010, **55**, 6332-6341.
114. W. Luo, C. F. Lin, O. Zhao, M. Noked, Y. Zhang, G. W. Rubloff and L. Hu, *Advanced Energy Materials*, 2016, **7**, 1601526.
115. P. Adelhelm, P. Hartmann, C. L. Bender, M. Busche, C. Eufinger and J. Janek, *Beilstein Journal of Nanotechnology*, 2015, **6**, 1016-1055.
116. Z. W. Seh, J. Sun, Y. Sun and Y. Cui, *ACS Cent Sci*, 2015, **1**, 449-455.
117. D. Aurbach, Y. Gofer, A. Schechter, O. Chusid, H. Gizbar, Y. Cohen, M. Moshkovich and R. Turgeman, *Journal of Power Sources*, 2001, **97-98**, 269-273.
118. D. Aurbach, R. Skaletsky and Y. Gofer, *Journal of The Electrochemical Society*, 1991, **138**, 3536.
119. C. Liebenow, *Journal of Applied Electrochemistry*, 1997, **27**, 221-225.
120. D. Aurbach, Z. Lu, A. Schechter, Y. Gofer, H. Gizbar, R. Turgeman, Y. Cohen, M. Moshkovich and E. Levi, *Nature*, 2000, **407**, 724-727.
121. T. Watkins, A. Kumar and D. A. Buttry, *Journal of the American Chemical Society*, 2016, **138**, 641-650.
122. S. B. Son, T. Gao, S. P. Harvey, K. X. Steirer, A. Stokes, A. Norman, C. Wang, A. Cresce, K. Xu and C. Ban, *Nat Chem*, 2018, **10**, 532-539.
123. K. A. See, J. A. Gerbec, Y.-S. Jun, F. Wudl, G. D. Stucky and R. Seshadri, *Advanced Energy Materials*, 2013, **3**, 1056-1061.
124. D. Wang, X. Gao, Y. Chen, L. Jin, C. Kuss and P. G. Bruce, *Nat Mater*, 2018,

- 17, 16-20.
125. A. Ponrouch, C. Frontera, F. Barde and M. R. Palacin, *Nat Mater*, 2016, **15**, 169-172.
126. S. Li, M. Jiang, Y. Xie, H. Xu, J. Jia and J. Li, *Adv Mater*, 2018, **30**, e1706375.
127. L. P. Hou, X. Q. Zhang, B. Q. Li and Q. Zhang, *Angewandte Chemie International Edition*, 2020, **59**, 15109-15113.
128. G. He, Q. Li, Y. Shen and Y. Ding, *Angewandte Chemie International Edition*, 2019, **58**, 18466-18470.
129. S. Xia, Q. Guo, Y. Yu, Y. Li, S. Wang, D. Dong, Z. Liu, H. Zhou, X. Zhou and Z. Liu, *Carbon*, 2023, **203**, 743-752.
130. S. Zhang, W. Deng, X. Zhou, B. He, J. Liang, F. Zhao, Q. Guo and Z. Liu, *Materials Today Energy*, 2021, **21**, 100770.
131. A. Aryanfar, D. J. Brooks, A. J. Colussi, B. V. Merinov, W. A. Goddard, 3rd and M. R. Hoffmann, *Physical Chemistry Chemical Physics*, 2015, **17**, 8000-8005.
132. P. Zou, Y. Sui, H. Zhan, C. Wang, H. L. Xin, H. M. Cheng, F. Kang and C. Yang, *Chemical Reviews*, 2021, **121**, 5986-6056.
133. P. Bai, J. Li, F. R. Brushett and M. Z. Bazant, *Energy & Environmental Science*, 2016, **9**, 3221-3229.
134. K. N. Wood, E. Kazyak, A. F. Chadwick, K. H. Chen, J. G. Zhang, K. Thornton and N. P. Dasgupta, *ACS Cent Sci*, 2016, **2**, 790-801.
135. F. Ding, W. Xu, G. L. Graff, J. Zhang, M. L. Sushko, X. Chen, Y. Shao, M. H. Engelhard, Z. Nie, J. Xiao, X. Liu, P. V. Sushko, J. Liu and J. G. Zhang, *Journal of The American Chemical Society* 2013, **135**, 4450-4456.
136. H. L. Skriver and N. M. Rosengaard, *Physical Review B*, 1992, **46**, 7157-7168.
137. C. Ling, D. Banerjee and M. Matsui, *Electrochimica Acta*, 2012, **76**, 270-274.
138. H. D. Yoo, I. Shterenberg, Y. Gofer, G. Gershinsky, N. Pour and D. Aurbach, *Energy & Environmental Science*, 2013, **6**, 2265-2279.
139. R. Davidson, A. Verma, D. Santos, F. Hao, C. Fincher, S. Xiang, J. Van Buskirk, K. Xie, M. Pharr, P. P. Mukherjee and S. Banerjee, *ACS Energy Letters*, 2018, **4**, 375-376.

140. M. Jackle and A. Gross, *J Chem Phys*, 2014, **141**, 174710.
141. J. H. Han, E. Khoo, P. Bai and M. Z. Bazant, *Sci Rep*, 2014, **4**, 7056.
142. H. J. S. Sand, *The London, Edinburgh, and Dublin Philosophical Magazine and Journal of Science*, 1901, **1**, 45-79.
143. L. Suo, Y. S. Hu, H. Li, M. Armand and L. Chen, *Nat Commun*, 2013, **4**, 1481.
144. L. Schafzahl, I. Hanzu, M. Wilkening and S. A. Freunberger, *ChemSusChem*, 2017, **10**, 401-408.
145. N. Xiao, W. D. McCulloch and Y. Wu, *J Am Chem Soc*, 2017, **139**, 9475-9478.
146. X. B. Cheng, R. Zhang, C. Z. Zhao and Q. Zhang, *Chemical Reviews*, 2017, **117**, 10403-10473.
147. B. Liu, J.-G. Zhang and W. Xu, *Joule*, 2018, **2**, 833-845.
148. Q. Pang, J. Meng, S. Gupta, X. Hong, C. Y. Kwok, J. Zhao, Y. Jin, L. Xu, O. Karahan, Z. Wang, S. Toll, L. Mai, L. F. Nazar, M. Balasubramanian, B. Narayanan and D. R. Sadoway, *Nature*, 2022, **608**, 704-711.
149. W. Brockner, K. Toerklep and H. A. Oeye, *Journal of Chemical & Engineering Data*, 1981, **26**, 250-253.
150. C. Wei, L. Tan, Y. Zhang, Z. Wang, B. Xi, S. Xiong, J. Feng and Y. Qian, *Energy Storage Materials*, 2022, **50**, 473-494.
151. H. Kim, D. A. Boysen, J. M. Newhouse, B. L. Spatocco, B. Chung, P. J. Burke, D. J. Bradwell, K. Jiang, A. A. Tomaszowska, K. Wang, W. Wei, L. A. Ortiz, S. A. Barriga, S. M. Poizeau and D. R. Sadoway, *Chemical Reviews*, 2013, **113**, 2075-2099.
152. V. Giordani, D. Tozier, H. Tan, C. M. Burke, B. M. Gallant, J. Uddin, J. R. Greer, B. D. McCloskey, G. V. Chase and D. Addison, *Journal of the American Chemical Society*, 2016, **138**, 2656-2663.
153. C. Xia, C. Y. Kwok and L. F. Nazar, *Science*, 2018, **361**, 777-781.
154. H. Yin, B. Chung, F. Chen, T. Ouchi, J. Zhao, N. Tanaka and D. R. Sadoway, *Nature Energy*, 2018, **3**, 127-131.
155. J. Prakash, L. Redey and D. R. Vissers, *Journal of Power Sources*, 1999, **84**, 63-69.

156. N. Shamim, E. C. Thomsen, V. V. Viswanathan, D. M. Reed, V. L. Sprenkle and G. Li, *Materials*, 2021, **14**, 2280.
157. Y. G. Zhu, G. Leverick, A. Accogli, K. Gordiz, Y. Zhang and Y. Shao-Horn, *Energy & Environmental Science*, 2022, **15**, 4636-4646.
158. D. J. Bradwell, H. Kim, A. H. C. Sirk and D. R. Sadoway, *Journal of the American Chemical Society*, 2012, **134**, 1895-1897.
159. H. Kim, D. A. Boysen, T. Ouchi and D. R. Sadoway, *Journal of Power Sources*, 2013, **241**, 239-248.
160. Y. Song, S. Jiao, J. Tu, J. Wang, Y. Liu, H. Jiao, X. Mao, Z. Guo and D. J. Fray, *Journal of Materials Chemistry A*, 2017, **5**, 1282-1291.
161. J. Tu, J. Wang, H. Zhu and S. Jiao, *Journal of Alloys and Compounds*, 2020, **821**, 153285.
162. S. Zhang, Y. Yang, L. Cheng, J. Sun, X. Wang, P. Nan, C. Xie, H. Yu, Y. Xia, B. Ge, J. Lin, L. Zhang, C. Guan, G. Xiao, C. Peng, G. Z. Chen and J.-Q. Wang, *Energy Storage Materials*, 2021, **35**, 142-147.
163. K. B. Hueso, M. Armand and T. Rojo, *Energy & Environmental Science*, 2013, **6**, 734-749.
164. K. Wang, Z. Chen, K. Liu, C. Yang, H. Zhang, Y. Wu, Y. Long, H. Liu, Y. Jin, M. Li and H. Wu, *Energy & Environmental Science*, 2022, **15**, 5229-5239.
165. Y. Wang, Y. Song and Y. Xia, *Chemical Society Reviews*, 2016, **45**, 5925-5950.
166. D. W. Kirk and J. W. Graydon, *ECS Transactions*, 2013, **53**, 27.
167. W. Zhao, H. Ren, T. Yan, Y. Ou, Q. Jiao, H. Wang, D. J. Kline and M. R. Zachariah, *Chemical Engineering Journal*, 2020, **396**, 124559.